Suppression of ACADM-mediated fatty acid oxidation promotes hepatocellular carcinoma via aberrant Cav1/SREBP-1 signaling

Angel P. Y. Ma[1], Cherlie L. S. Yeung[1], Sze Keong Tey[1], Xiaowen Mao[1], Samuel W. K. Wong[1], Tung Him Ng[1], Frankie C. F. Ko[1], Ernest M. L. Kwong[1], Alexander H. N. Tang[1], Irene Oi-Lin Ng[1,2], Shao Hang Cai[3], Jing Ping Yun[4], Judy W. P. Yam[1,2]

[1]Department of Pathology, Li Ka Shing Faculty of Medicine, The University of Hong Kong, Hong Kong, China.

[2]State Key Laboratory of Liver Research, The University of Hong Kong, Hong Kong, China.

[3]Department of Infectious Diseases, Nanfang Hospital, Southern Medical University, Guangzhou, China.

[4]Department of Pathology, Sun Yat-sen University Cancer Center, Guangzhou, China.

Running title

Aberrant ACADM-mediated fatty acid oxidation exacerbates HCC

Keywords

β-oxidation; Cancer cell metabolism; Drug synergism; Lipid metabolism; Liver cancer.

20

21 *Corresponding author*

22 Name: Judy Wai Ping Yam

23 Address: Room 08-001, Block T, Queen Mary Hospital, Pokfulam Road, Hong Kong, China.

24 Telephone: 852 2255 2681

25 Email: judyyam@pathology.hku.hk

26

27 *Conflict of interest*

28 The authors declare no potential conflicts of interest.

29

30 *Word count*

31 Abstract: 245, Text: 5280

32

33 *Number of Figures & Tables*

34 7 Figures

35

36

37

Abstract

Lipid accumulation exacerbates tumor development, as it fuels the proliferative growth of cancer cells. The role of medium-chain acyl-CoA dehydrogenase (ACADM), an enzyme that catalyses the first step of mitochondrial fatty acid oxidation, in tumor biology remains elusive. Therefore, investigating its mode of dysregulation can shed light on metabolic dependencies in cancer development. In hepatocellular carcinoma (HCC), ACADM was significantly underexpressed, correlating with several aggressive clinicopathological features observed in patients. Functionally, suppression of ACADM promoted HCC cell motility with elevated triglyceride, phospholipid and cellular lipid droplet levels, indicating the tumor suppressive ability of ACADM in HCC. Sterol regulatory element-binding protein-1 (SREBP-1) was identified as a negative transcriptional regulator of ACADM. Subsequently, high levels of caveolin-1 (Cav1) were observed to inhibit fatty acid oxidation, which revealed its role in regulating lipid metabolism. Cav1 expression negatively correlated with ACADM and its upregulation enhanced nuclear accumulation of SREBP-1, resulting in suppressed ACADM activity and contributing to increased HCC cell aggressiveness. Administration of an SREBP-1 inhibitor in combination with sorafenib elicited a synergistic anti-tumor effect and significantly reduced HCC tumor growth in vivo. These findings indicate that deregulation of fatty acid oxidation mediated by the Cav1/SREBP-1/ACADM axis results in HCC progression, which implicates targeting fatty acid metabolism to improve HCC treatment.

57

58

59 **Statement of Significance**

60 This study identifies tumor suppressive effects of ACADM in hepatocellular carcinoma and
61 suggests promotion of β-oxidation to diminish fatty acid availability to cancer cells could be
62 used as a therapeutic strategy.

63

64

65 **Introduction**

66 Primary liver cancer is one of the top leading cause of cancer-related deaths worldwide (1).
67 Among the different types, hepatocellular carcinoma (HCC) is the most common type
68 accounting for approximately 90% of the cases, with its incidence rate higher in developing
69 countries. The administration of vaccines against hepatitis B virus in newborns has contributed
70 to the decline of cancer incidence and mortality in Asia (2), however an increasing trend is
71 being observed in Western countries (3) along with the rise of non-viral HCC cases.

72

73 The alterations in fatty acid metabolism are increasingly recognised for their role in inducing
74 carcinogenesis. In rapidly proliferating cancer cells, carbons are hijacked from energy
75 production to synthesise fatty acids, which can be sourced either exogenously or from *de novo*

synthesis (4). Current literature cannot confirm whether the upregulation or downregulation of fatty acid oxidation (β-oxidation) contributes to HCC tumourigenesis, which may be due to the tumour heterogeneity nature of HCC. The expression of many β-oxidation-related genes was found to vary significantly between different patients (5). The upregulation of hypoxia inducible factor-1α inhibited β-oxidation, resulting in decreased reactive oxygen species and increased glycolysis to further facilitate HCC development (6). The evidence highlights the significant potential of targeting β-oxidation to treat HCC.

Medium-chain acyl-CoA dehydrogenase (ACADM) catalyses the first step of β-oxidation and is responsible for the breakdown of medium-chain fatty acids in the mitochondria. Medium-chain acyl-CoA dehydrogenase deficiency, caused by mutations in the ACADM gene, is the most common inherited metabolic disorder in Caucasians and thus signifying the profound influence of ACADM in metabolic diseases (7). Alteration of ACADM expression is found in subjects with cardiovascular, metabolic and non-alcoholic fatty liver diseases (8-10). However, the role of ACADM in human cancers has not been thoroughly studied. To our knowledge, the only functional study of ACADM performed in hepatoma cells was carried out where ACADM knockdown enhanced tumour growth (6). The regulation of ACADM expression has not been fully defined in other cancers (6,11-13), and little is known regarding this enzyme and HCC in literature.

This study aims to unravel the mechanisms involved with aberrant lipid metabolism and to define novel biomarkers of HCC progression. The results presented here provide innovative insights into the dysregulation of ACADM-mediated β-oxidation by oncogenic Caveolin-1 (Cav1) and sterol regulatory element-binding protein-1 (SREBP-1) to facilitate cancer development in HCC. With ACADM being a critical functional component in promoting β-oxidation, the establishment of its tumour suppressor role indicates its promising potential as a biomarker for HCC proliferation and metastasis. The mode of interplay between ACADM, SREBP-1 and Cav1 inspired an enhanced synergised treatment model which will not only benefit HCC patients, but also for treating other diseases arising from metabolic disorders.

Materials and Methods

Patient samples

Fifty pairs of human HCC and their corresponding non-tumourous samples were obtained during surgical resections from patients at Queen Mary Hospital (QMH), Hong Kong and were selected for analysing ACADM mRNA expression in this study. Paraffin-embedded HCC specimens were obtained from the archives of the Department of Pathology, Sun Yat-sen University Cancer Center (SYSUCC), Guangzhou, China. The patients neither received any

chemotherapy nor radiotherapy prior to the surgery. Informed written consent was obtained from all the patients. The use of human samples was approved by the Institutional Review Board of The University of Hong Kong/Hospital Authority Hong Kong West Cluster (HKU/HA HKW IRB) and the Institute Research Medical Ethics Committee of SYSUCC.

Tissue microarray

The tissue microarray slides were constructed using paired HCC and adjacent non-tumourous liver tissues. First, the marked areas on each sample were punched with the MiniCore® Excilone (MiniCore, U.K.) to yield tissue cores of 0.6 mm in diameter. Samples were then re-embedded, fixed with 4% paraformaldehyde before embedding in paraffin wax. Subsequently, the paraffin-embedded sections were cut into 4 μm-thick slices and mounted onto glass slides. After dewaxing, the slides were treated with 3% hydrogen peroxide in methanol and blocked using a biotin-blocking kit (DAKO, Germany). The slides were incubated with primary antibodies after blocking: ACADM (Abcam Cat# ab92461, RRID:AB_10563530) at 1:600 dilution for 50 minutes and SREBP-1 (Santa Cruz Biotechnology Cat# sc-13551, RRID:AB_628282) at 1:25 dilution overnight at 4°C. The slides were washed three times with 1× PBS before incubation with the biotinylated secondary antibodies for 1 hour, then the slides were stained with 3, 3'-diaminobenzidine tetrahydrochloride in solution (DAKO). Finally, the slides were counterstained with Mayer's haematoxylin and observed under a microscope for

analysis.

The stained samples were quantified without prior knowledge of corresponding patients' clinicopathological data. To quantify ACADM expression, each specimen was individually scored as 0 for negative, 1 for weak positive, 2 for moderate positive and 3 for strong positive. The proportion of positive-stained cells in total tumour cells was in percentages of 0, 50%, 80% and 100%. The histoscore (H-score) was calculated by multiplying the percentage of positive cells with the score of intensity, giving a range of 0 to 300. To assess the nuclear immunoreactivity of SREBP-1, the percentage and intensity of nuclear signal were scored.

Cell cultures

The human HCC cell lines used in this study were either purchased from the American Type Culture Collection (Manassas, VA, USA) (Hep3B (ATCC Cat# HB-8064, RRID:CVCL_0326) and PLC/PRF/5 (ATCC Cat# CRL-8024, RRID:CVCL_0485)) or were sourced from the Cancer Institute, Fudan University, China (LM3 (RRID:CVCL_6832) and MHCC97L (RRID:CVCL_4973)), the Japanese Collection of Research Bioresources (Huh7 (JCRB Cat# JCRB0403, RRID:CVCL_0336) and HLE (JCRB Cat# JCRB0404, RRID:CVCL_1281)) and from Jayanta Roy-Chowdhury, Albert Einstein College of Medicine, New York (MIHA (RRID:CVCL_SA11)). All cell lines were cultured in Dulbecco's Modified Eagle Medium,

High Glucose supplemented with 10% fetal bovine serum (FBS) (Gibco), with the medium's final pH adjusted to 7. Cell cultures were kept in humidified incubators maintained at 37°C with 5% CO_2. Mycoplasma detection in cell cultures were carried out by PCR screening with primers Myco5 and Myco3 (Supplementary Table 1). Cell line authentication was performed by short tandem repeat DNA profiling (Bio-Gene).

Stable cell lines and expression constructs

To establish stable knockdown cells of Cav1 and ACADM, MISSION^{TM} short hairpin RNAs (shRNA) targeting Cav1 and ACADM and non-target control (CTL) were purchased from Sigma-Aldrich. To establish double knockdown cells of Cav1 and ACADM, shRNA targeting ACADM was subcloned into pLKO.1-Blast vector (RRID:Addgene_26655) via AgeI and EcoRI sites. To establish ACADM knockout in murine cells, single guide RNAs (sgRNA) targeting murine ACADM and the control sgRNAs (Integrated DNA Technologies) were synthesised and subcloned into the pX330-U6-Chimeric_BB-CBh-hSpCas9 vector (RRID:Addgene_42230). The sequences of oligos used in the study are provided in Supplementary Table 1. For stable overexpression of SREBP-1 cells, the human open reading frame (ORF) cDNA of SREBP-1 was purchased from Sino Biological (Cat. No. HG17512-UT). The plasmids were subjected to DNA sequencing carried out by the Centre for Genomic Sciences, HKU, to confirm the correct orientation and sequence of the insert in the plasmid.

Expression constructs were transfected into 293FT cells (ATCC Cat# PTA-5077, RRID:CVCL_6911) using the GeneCopoeia Lenti-Pac™ HIV expression packaging system; detailed procedures are described elsewhere (14).

Lipid detection assays

The EnzyChrom™ Triglyceride Assay Kit and Phospholipid Assay Kit (BioAssay Systems) were used to detect the level of triglycerides and phospholipids in cells. The manufacturer's protocol was followed, the experiments were done in triplicates and 1×10^6 cells were used per sample per well. Total cell lysate was used for sample normalisation.

Nile Red is a phenoxazone dye used to detect intracellular lipid droplets. Cells were prepared as follows: a clean coverslip was placed into a 6-well plate. An optimal number of cells was seeded into the well and incubated overnight at 37°C. The cells were gently rinsed with 1× PBS before fixing with 4% paraformaldehyde, staining with Nile Red (10 μg/ml, Sigma-Aldrich), then counterstaining with DAPI (Invitrogen). The coverslips were carefully mounted onto a clean glass slide with mounting medium (Vectashield). Cells were then visualised with confocal microscopy (Carl Zeiss LSM-700). Quantification of the signals was performed with the ImageJ software (ImageJ, RRID:SCR_003070) by normalising the Nile Red signal intensity with the DAPI signal, the latter of which indicate the nuclear staining level of the cells.

Oil Red O (Sigma) is a lysochrome diazo dye used for staining neutral triglycerides and lipids on frozen tissue sections. Briefly, fresh frozen tissue was cut into 5-10 μm thick sections and mounted on slides. The slides were then air-dried, fixed in ice-cold 10% formaldehyde, rinsed in distilled water and allowed to air-dry again before being placed in absolute propylene glycol to avoid carrying water into the Oil Red O. The staining was performed in pre-warmed Oil Red O solution, then differentiated in 85% propylene glycol solution. The slides were rinsed in distilled water, stained with haematoxylin, washed thoroughly under running tap water, placed in distilled water, then finally mounted with mounting medium.

Chromatin immunoprecipitation (ChIP)

The EpiQuik™ Chromatin Immunoprecipitation Kit (Epigenetik) was used to determine the interaction between SREBP-1 and the endogenous promoter of ACADM. The manufacturer's protocol was followed and PCR was performed to observe for any protein-DNA interactions. The sequences of primers ACADM-540F and ACADM+41R flanking the SREBP-1 binding site, and the primers ACADM-1450-F and ACADM-950-R flanking the -1450 to -950 region of the ACADM promoter are shown in Supplementary Table 1.

Hydrodynamic injection in FVB/N mice

The hydrodynamic tail vein injection was employed to induce transfection of foreign DNA inside the livers of mice. The following plasmids were used in this study: pT3-EF1-NRAS, pX330-TP53, Sleeping Beauty (SB) transposon and ACADM-KO. Plasmids were amplified using the GenElute^{TM} HP Endotoxin-Free Plasmid Maxiprep Kit (Sigma) according to the manufacturer's protocol. To prepare the plasmid solution for injection, 20 μg of each oncogene and 1.6 μg of SB transposon were used for each mouse. The plasmids were added to 1× PBS resulting in a total volume of 2 ml per mouse. The plasmid solution was then filtered through a 0.22 μm filter before use.

Immunocompetent male 6-week-old FVB/N mice (MGI Cat# 3528175, RRID:MGI:3528175) were selected for this procedure. Each mouse was placed in a mouse restrainer, then its tail was swabbed with 70% ethanol prior to injection. The plasmid solution was injected via the tail vein within 5-8 seconds. The mouse was then returned to its cage. Mouse weight was recorded biweekly until the mouse has reached its humane endpoint, at which point the liver was harvested and fixed in 10% formaldehyde for immunohistochemical staining. Antibodies used in this study are listed in Supplementary Table 2.

Drug treatment of cells

Etomoxir (ETO), an irreversible carnitine palmitoyl transferase 1 (CPT1)-specific inhibitor

228 which inhibits fatty acid entry into the mitochondrial matrix for β-oxidation, was used to treat
229 MHCC97L Cav1 knockdown cells. Cells were incubated with 100 μM of ETO (Cayman
230 Chemical) in the culture medium for 48 hours before being subjected to further experiments.
231
232 *Subcutaneous injection and drug treatment of nude mice*
233 Male BALB/cAnN-nu (Nude) mice of approximately 4-5 weeks of age were selected for
234 subcutaneous implantation of HCC cells to observe their tumourigenic ability. Various stably-
235 transfected HCC cell lines were subcutaneously injected into the flank of mice, with the optimal
236 cell number of each cell line suspended in 100 μl of either 1× PBS or Matrigel per injection.
237 The tumour sizes were measured using a calliper and monitored at the indicated time points
238 throughout the experiment, with the tumour volume calculated with the formula: 1/2 (largest
239 diameter) × (smallest diameter)^2. At the experimental endpoint, the mice were sacrificed before
240 tumours were excised and weighed.
241
242 For drug treatment, subcutaneous xenografts of 5 × 10^6 MHCC97L cells were injected into 4-
243 week-old nude mice. When the tumours reached 5 mm in diameter, mice were randomly
244 assigned to one of four groups and drugs were administered in the following combinations: (1)
245 vehicle, (2) eicosapentaenoic acid (EPA) (200 mg/kg), (3) sorafenib (30 mg/kg), and (4) EPA
246 + sorafenib. Both drugs were fed to mice via oral gavage in volumes of 100 μl, with sorafenib

fed daily for 21 days and EPA fed every other day for 10 days. Mouse weights and tumour sizes were recorded daily. At the experimental endpoint, the tumours were excised and weighed.

All mice in this study were fed with standard chow and raised in individually ventilated cages equipped with local woodchip for bedding. All experiments involving live animals were performed according to the Animals (Control of Experiments) Ordinance (Hong Kong), and the Institute's guidance from Laboratory Animal Unit on animal experimentation was strictly followed.

Clinicopathological correlation and statistical analysis

For the genes investigated in this study, their mRNA levels were correlated to various clinicopathological parameters in HCC patients using IBM SPSS statistics 20 (SPSS, RRID:SCR_002865). The parameters were determined and analysed by clinical pathologists upon surgical resection. Student's t-test, Kaplan-Meier analysis, log-rank test, Chi-squared test and Mann-Whitley U test were incorporated into the statistical analyses of data. All other statistical analyses were performed by GraphPad Prism 7 (GraphPad Prism, RRID:SCR_002798) where Student's t-test was used for the functional *in vitro* assays unless otherwise stated. $P < 0.05$ was considered as statistically significant.

Results

Clinical significance of ACADM downregulation in HCC

The mRNA expression of ACADM was analysed in 50 paired cases of HCC and their corresponding non-tumourous tissues from the QMH cohort. It was observed that ACADM was underexpressed in 64% (32/50) of HCC cases (Fig. 1A). The overall ACADM level was significantly lower in tumourous versus non-tumourous tissues; ACADM expression data from The Cancer Genome Atlas (TCGA) database also revealed a significant decrease in ACADM expression in tumourous samples (Fig. 1B). ACADM expression was found to be reduced with further HCC progression (Fig. 1C); its underexpression significantly correlated with the aggressive pathological features such as bigger tumour size, presence of venous invasion, advanced HCC tumour stage and poor cell differentiation (Fig. 1D & Supplementary Table 3). Receiver operating characteristic curves indicate the significant discrimination of ACADM expression between non-tumourous and early stage, but not between early and late stage HCC (Supplementary Fig. 1A-1B). Furthermore, ACADM expression was analysed in the SYSUCC cohort using tissue microarray. Immunohistochemical staining of ACADM protein expression in paired HCC tissues was scored as strong (45/51) and moderate (6/51) positive in 100% of non-tumourous liver tissues, when compared to strong and moderate positive in 52.9% (27/51) of tumourous tissues. Weak positive and negative were observed in 47.1% (24/51) of

tumourous tissues (Fig. 1E). Among 51 cases, ACADM was downregulated in 86.3% (44/51) of HCC tumours when compared to the adjacent non-tumourous liver tissues (Fig. 1F). Together, these findings indicate that the reduced ACADM level in tumourous tissues could be a valuable biomarker of HCC.

ACADM knockdown enhances cell aggressiveness in HCC

To functionally characterise ACADM in HCC, it was suppressed in non-metastatic Huh7 cells. Stable non-target control and ACADM knockdown clones (shACADM; sh61 and sh65) were established and verified with western blot (Fig. 2A). ACADM knockdown enhanced cellular lipid content, triglycerides and phospholipids in shACADM compared to the shCTL cells (Fig. 2B), with similar results observed in immortalised normal liver cell line MIHA (Supplementary Fig. 2A-2B). As reflected by the cellular respiration rate, shACADM cells displayed reduced fatty acid oxidation when compared to shCTL cells (Fig. 2C). Fatty acid profiling revealed the overall increase in fatty acids in shACADM cells, with the same being observed in both palmitic acid and oleic acid levels (Fig. 2D). The abundance of other saturated and unsaturated fatty acids was found to be elevated in shACADM cells compared to shCTL (Supplementary Fig. 3A-3B). Diminution of ACADM in Huh7 and MIHA cells significantly encouraged cell growth, anchorage independent growth, migration and invasiveness of the shACADM cells, indicating their enhanced cell aggressiveness compared to the shCTL (Fig. 2E and

304 Supplementary Fig. 4A-4B). The tumour development rate significantly increased in
305 subcutaneous xenografts derived from shACADM cells (Fig. 2F), with immunohistochemical
306 staining indicating the higher proliferation rate of shACADM cells compared to the shCTL
307 (Fig. 2G).
308
309 The oncogenic effect of ACADM knockdown was further analysed by hydrodynamic injection
310 mouse model. ACADM expression was found to correlate to NRAS/p53 gene alterations
311 according to the TCGA database (Supplementary Fig. 5A). The establishment of the ACADM-
312 KO plasmids (ACADM-KO1 and ACADM-KO2) were confirmed in murine NIH3T3 cells
313 with western blot (Supplementary Fig. 5B). Plasmids used in the experiment and the
314 approximate timeline of actions were depicted, with the mice split into three groups to observe
315 the effect of different oncogenic plasmid combinations on HCC development (Fig. 2H). At
316 week 4 post-injection, larger tumours were formed in mice injected with the N-RasV12, p53-
317 and ACADM-KO plasmids versus mice without ACADM-KO plasmid (Supplementary Fig.
318 5C). At the end of the experiment, it was observed that injection with ACADM-KO plasmid
319 resulted in significantly more tumour formation and larger tumour sizes compared to either the
320 control group or the mice only injected with RasV12 and p53-KO plasmids (Fig. 2H).
321 Nevertheless, significant differences were not observed between the end-point liver weight,
322 liver:body weight ratio and mouse weight of mice injected with RasV12 and p53-KO plasmids

with or without ACADM-KO plasmid (Supplementary Fig. 5D). Immunohistochemical staining of the excised livers revealed the ACADM knockout expression and N-Ras overexpression in mice that received injection of ACADM-KO and RasV12 plasmids (Fig. 2I). The expression of p53 was not detected in the normal liver; in mice injected with p53-KO plasmid, p53 was not detected in tumour cells but observed in adjacent lymphoid cells suggesting the successful knockout of p53 in tumours.

SREBP-1 is the direct upstream regulator of ACADM in HCC

To determine how ACADM is regulated in HCC, the activity of ACADM promoter in cells was investigated. Submitting the ACADM promoter sequence to MatInspector (Genomatrix) revealed two putative transcription factor binding sites upstream of the ACADM transcription site, peroxisome proliferator response element (PPRE) and sterol regulatory element (SRE). To confirm whether these two sites play a significant role in regulating ACADM transcription, both sites were mutated. In MHCC97L cells, high ACADM promoter activity was observed for the SRE-mutant versus the wildtype ACADM promoter (-1450), with the non-significance between the PPRE-mutant and the wildtype promoter. SRE is the binding site of SREBP-1; RT-qPCR using primers flanking SRE but not primers amplifying unrelated region of ACADM promoter revealed the increased copy number of ACADM promoter fragments pulled down by anti-SREBP-1 antibody in MHCC97L cells (Fig. 3A). These findings suggested that SREBP-

1 is a negative regulator of ACADM.

Inversely correlated expressions of SREBP-1 and ACADM in HCC

To determine the clinical relevance of SREBP-1 and ACADM in HCC, we examined their expressions in a cohort of HCC tissues from SYSUCC (n = 41). The SREBP-1 expression was inversely correlated with ACADM expression with significance; in cases with SREBP-1 overexpression, reduced levels of ACADM were detected in tumourous tissues (Fig. 3B). In tissue microarray comprising of 46 HCC specimens, strong and moderate positive staining of SREBP-1 were detected in 41.3% (19/46) of tumourous tissues while only weak positive and negative were detected in non-tumourous tissues (Fig. 3C; Supplementary Fig. 6). The nuclear immunoreactivity of SREBP-1 was significantly higher in tumourous tissues as indicated by the higher H-score. The overall SREBP-1 expression was higher in tumourous tissues when compared to non-tumourous tissues, and SREBP-1 overexpression was found in 56.5% (26/46) of the cases (Fig. 3C). These data established the association between ACADM underexpression and SREBP-1 upregulation in human HCC.

Cav1 enhances SREBP-1 nuclear accumulation to suppress ACADM

Since SREBP-1 has previously been reported to interact with Cav1 in other diseases (15,16), this warrants further investigation into their interplay in HCC. It was revealed that the ACADM

promoter activity was significantly elevated in shCav1 cells (Fig. 3D). It was observed that a lower Cav1 level prevented the nuclear accumulation of SREBP-1 and enhanced ACADM expression in MHCC97L shCav1 cells, with treatment of filipin, a Cav1 inhibitor (17), inducing the same effect in MHCC97L shCTL cells (Fig. 3E). The results implicate that Cav1 facilitates nuclear accumulation of SREBP-1 leading to the negative transcriptional regulation of ACADM. Restoration of SREBP-1 in MHCC97L shCav1 cells reduced ACADM expression (Fig. 3F). Conversely, knockdown of SREBP-1 upregulated ACADM level in MHCC97L cells (Fig. 3G). Our data also showed that Cav1 interacted with full-length SREBP-1 in MHCC97L cells, implicating the potential role of Cav1 to mediate the maturation and nuclear accumulation of SREBP-1 (Supplementary Fig. 7). Further investigation will be needed to delineate how Cav1 regulates the activation of SREBP-1 leading to ACADM downregulation.

Cav1 promotes HCC progression in part by modulating β-oxidation

Literature has revealed the emerging roles of Cav1 in cancer metabolism (18-20). However, its mode of action remains unclear, especially in cancer. To investigate the prospective role of Cav1 in β-oxidation, an examination of the effect of Cav1 on cellular lipid levels was conducted in metastatic MHCC97L cells. First, stable non-target control (shCTL) and Cav1 knockdown (shCav1) clones were established (Fig. 4A). The knockdown of Cav1 significantly reduced the cellular triglycerides, phospholipids and lipid accumulation levels compared to the shCTL cells

(Fig. 4B). The oxygen consumption rate increased in shCav1 cells, indicating the increase in β-oxidation compared to the shCTL (Fig. 4C). The same effects were observed in non-metastatic Hep3B cells (Supplementary Fig. 8A-8C), suggesting that Cav1 can downregulate β-oxidation.

Cav1 enhances HCC cell aggressiveness by suppressing β-oxidation

Since Cav1 exerts potent effects in driving HCC tumourigenesis and metastasis, it is intriguing whether an alteration in β-oxidation contributes to the oncogenic properties of Cav1. Etomoxir (ETO) treatment inhibited fatty acid breakdown and resulted in the restoration of triglycerides, phospholipids and lipid droplets in shCav1 cells (Fig. 4D). Cav1 knockdown significantly diminished the proliferation rate, anchorage-independent growth, migration and invasiveness of MHCC97L cells; however, such diminishment was partly restored in shCav1 cells treated with ETO (Fig. 4E), with the same effect observed in Hep3B cells (Supplementary Fig. 8D). The cell aggressiveness was also augmented in nude mice intraperitoneally injected with ETO, with immunohistochemistry indicative of the Cav1 expression and Oil Red O staining revealing the build-up of oil droplets in shCav1 tumours treated with ETO compared to the non-treated tumours (Fig. 4F). To demonstrate the functional interaction between Cav1 and SREBP-1, SREBP-1 was overexpressed in MHCC97L Cav1 knockdown cells; the enhancement of fatty acid oxidation in shCav1 cells was suppressed by SREBP-1 overexpression (Fig. 4G).

399 Functionally, the reduced promoting function of Cav1 was rescued by overexpressing SREBP-
400 1 in shCav1 cells; these cells displayed increased anchorage independent growth, cell migration
401 and invasion (Fig. 4H).
402
403 *Negative correlation between Cav1 and ACADM*
404 To investigate whether Cav1 correlates with ACADM in HCC, their mRNA and protein
405 expression levels were analysed. In the HCC cell line panel, ACADM and Cav1 expressions
406 were found to be negatively correlated (Fig. 5A & 5B). Immunohistochemistry revealed the
407 alternated expressions of Cav1 and ACADM in tumours derived from MHCC97L cells
408 implanted into the mouse liver (Fig. 5C). The enhanced transcriptional and protein levels of
409 ACADM were also validated in both Hep3B and MHCC97L shCav1 cells (Fig. 5D & 5E). The
410 mRNA expressions of ACADM and Cav1 in 25 paired clinical samples of HCC and non-
411 tumourous tissues from QMH were determined; consistent with their association observed in
412 cell lines, their negative correlation was also observed to be significant in data obtained from
413 the TCGA database (Fig. 5F).
414
415 *Suppression of ACADM in shCav1 cells restores HCC aggressiveness*
416 To validate whether Cav1 mediates β-oxidation via ACADM in HCC, ACADM was suppressed
417 in shCav1 MHCC97L and Hep3B cells to recapitulate the functional effect of Cav1

418 overexpression (Fig. 6A). The resulting effects were that the levels of triglycerides,
419 phospholipids, intracellular lipid contents as well as fatty acid oxidation were elevated in
420 double knockdown cells of Cav1 and ACADM (shCav1/sh61 and shCav1/sh65) (Fig. 6B-6D).
421 The enhancement of HCC anchorage independent growth, cell growth and motility were also
422 observed in the double knockdown cells compared to the shCav1 cells (Fig. 6E - 6G). The same
423 effect was observed in animal models, with the shCav1/sh61 tumours proliferating much
424 quicker than the shCav1 only tumours (Fig. 6H); immunohistochemical staining revealed the
425 darker staining of CD31 and Ki67 in shCav1/sh61 tumours, highlighting the elevated
426 angiogenesis and cell proliferation rates compared to the shCav1 only cells (Fig. 6I).
427
428 *SREBP-1 antagonist enhances the efficacy of sorafenib and suppresses HCC development*
429 Based on the *in vitro* findings, we hypothesised that the inhibition of fatty acid synthesis genes
430 can potentially inhibit the proliferation of cancer cells. EPA was found to inhibit the maturation
431 of SREBP-1 protein in hepatocytes (21). Reduction of activated SREBP-1 was observed in
432 MHCC97L cells after EPA treatment (Fig. 7A). The therapeutic effect of EPA alone and in
433 combination with sorafenib was investigated in MHCC97L subcutaneous xenograft mouse
434 model (Fig. 7B). The significant efficacy enhancement of the combinational treatment of
435 sorafenib with EPA to suppress HCC growth was observed (Fig. 7C). Significant reductions in
436 tumour volume and weight were also observed in the combinational treatment group compared

437 to single administrations of either drug (Fig. 7D). Animals treated with drugs did not reveal
438 significant weight loss when compared to animals of other groups (Supplementary Fig. 9).
439 Tumours treated with EPA alone or in combination with sorafenib resulted in the decrease in
440 SREPB-1 and increase in ACADM expressions (Fig. 7E). Tumours formed in mice which
441 received the combined treatment showed the least Ki67 staining among the four experimental
442 groups.
443
444
445 **Discussion**
446 Despite a previous report of using Hep3B cells to investigate the role of ACADM in tumour
447 growth (6), the demonstration of its role in HCC metastasis is still deficient. In this study,
448 ACADM knockdown remarkably enhanced lipid accumulation and cell aggressiveness *in vitro*,
449 while ACADM knockout modulated the tumour growth in mice, suggesting that the loss of
450 ACADM augmented HCC aggressiveness and that ACADM is a functional component in
451 promoting β-oxidation. Although a non-significant difference in ACADM expression between
452 HCC lesions and adjacent normal tissues was previously reported (6), our data showed that
453 ACADM was underexpressed in the vast majority of HCC patients. Altogether, the results
454 highlighted ACADM's potential as a valuable biomarker during HCC development.
455

456 The mutation of the SRE binding site, which substantially boosted ACADM expression in HCC
457 cells, suggested that genes binding to SRE are responsible for controlling ACADM expression.
458 SRE is the transcription factor binding site of SREBPs, which are cholesterol sensors located
459 in the endoplasmic reticulum (ER) that regulate intracellular cholesterol (22) and fatty acid
460 synthesis (23). SREBP-1c is one of the three isoforms of SREBPs that is mainly found in the
461 liver, muscles and fat tissues (24). In cancer cells, the frequent overexpression of SREBPs
462 resulted in the accumulation of lipids to enhance cell proliferation rate (25). In this study, the
463 previously unprecedented suppression of ACADM by SREBP-1 prevented β-oxidation,
464 leading to further lipid accumulation to fuel cancer growth; our observation corroborates with
465 other findings that SREBP-1 overexpression can suppress various lipid oxidation genes in
466 bovine hepatocytes (26,27).
467
468 The precursor form of SREBP-1 resides in the ER; upregulation of SREBP-1 leads to lipid
469 accumulation in normal hepatic and hepatoma cells under ER stress (28). Though normally
470 localised to the plasma membrane, Cav1 has been shown to accumulate in the ER which causes
471 the protein to be targeted to lipid droplets (29), therefore it is possible for Cav1 to interact with
472 the precursor of SREBP-1 in the ER. Although previously reported to interact with each other
473 in other cancers, the interplay of SREBP-1 and Cav1 remained ambiguous in HCC. Here, Cav1
474 was revealed to be a positive regulator of SREBP-1 by acting upstream to modulate SREBP-1

475 expression in HCC. The overexpression of SREBP-1 in Cav1 knockdown cells did not affect
476 Cav1 expression, but restored their cell aggressiveness, which confirmed the positive
477 correlation between these two genes. However, how Cav1 facilitates SREBP-1 nuclear
478 accumulation remains unclear. The transcriptional increase in ACADM expression was
479 detected upon the knockdown of Cav1. Pooling together these results, they indicate that Cav1
480 can modulate fatty acid metabolism via the activation of SREBP-1 to suppress ACADM in
481 HCC.
482
483 The oncogenic role of Cav1 in cancer has been well established; it is an important factor
484 involved in tumourigenesis and progression of many cancers, but with context dependent
485 functions. Our previous study demonstrated the definitive role of Cav1 in HCC metastasis, also
486 revealing the dramatic expression of Cav1 in metastatic HCC cells (14). The upregulation of
487 Cav1 associated with the presence of C-terminal truncated HBx in HCC, which activates the
488 transcription of Cav1 with significant functional impact on HCC tumourigenesis (30). Based
489 on the knowledge that metastasis is a prominent feature in the advanced stage of HCC and that
490 Cav1 is a potent metastasis promoter, the role of ACADM as an effector of Cav1 was explored.
491 Compared to other β-oxidation genes, ACADM was of particular interest due to how its
492 oxidation target, medium-chain fatty acids (C6 - C12), has the ability to diffuse unaided into
493 the mitochondria as opposed to longer-chain fatty acids which have to be imported by CPT1;

494 this is due to the increased solubility of shorter-chain fatty acids into the mitochondrial
495 membrane (31). This diversion from the carnitine shuttle may reveal a previously unrecognised
496 pathway that bypasses CPT1 to regulate β-oxidation. We speculated that Cav1 regulates β-
497 oxidation by inhibiting ACADM expression, which was proven by the negative correlation of
498 Cav1 and ACADM in HCC cellular models, animal models and patient biopsies.
499
500 As a routine medication used to treat unresectable HCC, sorafenib is an important multikinase
501 inhibitor drug which is also applied for the treatment of several other types of cancers, although
502 its effect on prolonging the survival of patients for only a few months leaves a lot to be desired.
503 From previous reports, it can be theorised that by targeting SREBP1 activity, it will inhibit the
504 expression of fatty acid synthesis genes which can potentially inhibit the proliferation of cancer
505 cells. EPA is a major component of ω-3 polyunsaturated fatty acids which can enhance fatty
506 acid oxidation and reduce *de novo* lipogenesis by modulating transcription factors to inhibit
507 SREBP-1 nuclear translocation (32,33); it has previously been shown to inhibit SREBP-1
508 activity by inhibiting its nuclear translocation in hepatocytes (21,34). In normal cells, the
509 overabundance of unsaturated fatty acids triggers a negative feedback loop, which suppresses
510 SREBP-1c expression to prevent excessive lipid accumulation (35). The administration of EPA
511 in combination with another omega-3 fatty acid, docosahexaenoic acid (DHA), have been
512 shown to alleviate illness and to promote general good health in mice (36), with the enhanced

protective effect of EPA over DHA highlighted (37). Here, we showed that the combinational treatment of EPA and sorafenib markedly suppressed the growth of MHCC97L subcutaneous xenografts when compared to treatments with either drug alone. This phenomenon can be attributed to the broad-spectrum protein kinase inhibitor activity of EPA previously observed in both prostate and breast cancers (38,39), which further enhanced the multikinase inhibitor and anti-tumour properties of sorafenib. Therefore, our data indicates the immense potential of the co-administration of EPA and sorafenib in slowing down HCC progression to provide a better prognosis for patients.

In conclusion, this study has revealed the mode of ACADM-mediated fatty acid oxidation in HCC and how its dysregulation led to the increase in fatty acid availability for promoting the proliferation and metastatic abilities of HCC cells (Fig. 7F). We highlighted the critical function of ACADM as a tumour suppressor in its role of modulating fatty acid metabolism to inhibit tumourigenesis and HCC development, which indicate its potential as a biomarker for HCC proliferation and metastasis. Our data delineated the novel Cav1/SREBP-1/ACADM axis in the regulation of fatty acid oxidation in HCC, and revealed the immense therapeutic potential of suppressing SREBP-1 activity to synergise sorafenib potency in treating HCC. All in all, this study has contributed to a better understanding of the mechanistic pathways that shape the dysregulation of fatty acid metabolism in HCC, which will be beneficial to the advancement

of targeted therapies for cancer patients, since tumour metabolism plays such a key role in cancer development.

Acknowledgements

This work is supported by the Hong Kong Research Grants Council, General Research Fund (Project number: 17100418) and the University Research Committee, Seed Fund for Basic Research (Project number: 201711159021). IOL is Loke Yew Professor in Pathology. We would like to thank Dr Rakesh Sharma at the Proteomics and Metabolomics Core Facility, LKS Faculty of Medicine, HKU for conducting the fatty acid profiling. Imaging data were acquired using equipment maintained by the Imaging and Flow Cytometry Core, Center for PanorOmic Sciences, LKS Faculty of Medicine, HKU.

References

1. Bray F, Ferlay J, Soerjomataram I, Siegel RL, Torre LA, Jemal A. Global cancer statistics 2018: GLOBOCAN estimates of incidence and mortality worldwide for 36 cancers in 185 countries. CA: a cancer journal for clinicians **2018**;68:394-424
2. Chen W, Zheng R, Baade PD, Zhang S, Zeng H, Bray F*, et al.* Cancer statistics in China,

2015. CA: a cancer journal for clinicians **2016**;66:115-32

3. Siegel RL, Miller KD, Jemal A. Cancer statistics, 2019. CA: a cancer journal for clinicians **2019**;69:7-34

4. Medes G, Thomas A, Weinhouse S. Metabolism of neoplastic tissue. IV. A study of lipid synthesis in neoplastic tissue slices in vitro. Cancer research **1953**;13:27-9

5. Björnson E, Mukhopadhyay B, Asplund A, Pristovsek N, Cinar R, Romeo S*, et al.* Stratification of Hepatocellular Carcinoma Patients Based on Acetate Utilization. Cell reports **2015**;13:2014-26

6. Huang D, Li T, Li X, Zhang L, Sun L, He X*, et al.* HIF-1-Mediated Suppression of Acyl-CoA Dehydrogenases and Fatty Acid Oxidation Is Critical for Cancer Progression. Cell reports **2014**;8:1930-42

7. Oerton J, Khalid JM, Besley G, Dalton RN, Downing M, Green A*, et al.* Newborn screening for medium chain acyl-CoA dehydrogenase deficiency in England: prevalence, predictive value and test validity based on 1.5 million screened babies. J Med Screen **2011**;18:173-81

8. Van Berendoncks AM, Garnier A, Beckers P, Hoymans VY, Possemiers N, Fortin D*, et al.* Exercise training reverses adiponectin resistance in skeletal muscle of patients with chronic heart failure. Heart (British Cardiac Society) **2011**;97:1403-9

9. Simula MP, Cannizzaro R, Canzonieri V, Pavan A, Maiero S, Toffoli G*, et al.* PPAR

570 signaling pathway and cancer-related proteins are involved in celiac disease-associated
571 tissue damage. Molecular medicine (Cambridge, Mass) **2010**;16:199-209
572 10. Mitsuyoshi H, Yasui K, Harano Y, Endo M, Tsuji K, Minami M*, et al.* Analysis of hepatic
573 genes involved in the metabolism of fatty acids and iron in nonalcoholic fatty liver
574 disease. Hepatology research : the official journal of the Japan Society of Hepatology
575 **2009**;39:366-73
576 11. Seok S, Kim YC, Byun S, Choi S, Xiao Z, Iwamori N*, et al.* Fasting-induced JMJD3
577 histone demethylase epigenetically activates mitochondrial fatty acid β-oxidation. The
578 Journal of clinical investigation **2018**;128:3144-59
579 12. Wu Y, Sarkissyan M, McGhee E, Lee S, Vadgama JV. Combined inhibition of glycolysis
580 and AMPK induces synergistic breast cancer cell killing. Breast Cancer Res Treat
581 **2015**;151:529-39
582 13. Sohn EJ, Kim J, Hwang Y, Im S, Moon Y, Kang DM. TGF-β suppresses the expression
583 of genes related to mitochondrial function in lung A549 cells. Cellular and molecular
584 biology (Noisy-le-Grand, France) **2012**;Suppl.58:Ol1763-7
585 14. Tse EY, Ko FC, Tung EK, Chan LK, Lee TK, Ngan ES*, et al.* Caveolin-1 overexpression
586 is associated with hepatocellular carcinoma tumourigenesis and metastasis. The Journal
587 of pathology **2012**;226:645-53
588 15. Yeh M, Cole AL, Choi J, Liu Y, Tulchinsky D, Qiao JH*, et al.* Role for sterol regulatory

element-binding protein in activation of endothelial cells by phospholipid oxidation products. Circulation research **2004**;95:780-8

16. Prade E, Tobiasch M, Hitkova I, Schaffer I, Lian F, Xing X*, et al.* Bile acids down-regulate caveolin-1 in esophageal epithelial cells through sterol responsive element-binding protein. Mol Endocrinol **2012**;26:819-32

17. Xu Y, Henning RH, van der Want JJL, van Buiten A, van Gilst WH, Buikema H. Disruption of endothelial caveolae is associated with impairment of both NO- as well as EDHF in acetylcholine-induced relaxation depending on their relative contribution in different vascular beds. Life Sciences **2007**;80:1678-85

18. Mastrodonato M, Calamita G, Rossi R, Mentino D, Bonfrate L, Portincasa P*, et al.* Altered distribution of caveolin-1 in early liver steatosis. European journal of clinical investigation **2011**;41:642-51

19. Asterholm IW, Mundy DI, Weng J, Anderson RG, Scherer PE. Altered mitochondrial function and metabolic inflexibility associated with loss of caveolin-1. Cell metabolism **2012**;15:171-85

20. Fernández-Rojo MA, Restall C, Ferguson C, Martel N, Martin S, Bosch M*, et al.* Caveolin-1 orchestrates the balance between glucose and lipid-dependent energy metabolism: implications for liver regeneration. Hepatology (Baltimore, Md) **2012**;55:1574-84

608 21. Tanaka N, Zhang X, Sugiyama E, Kono H, Horiuchi A, Nakajima T*, et al.*
609 Eicosapentaenoic acid improves hepatic steatosis independent of PPARα activation
610 through inhibition of SREBP-1 maturation in mice. Biochem Pharmacol **2010**;80:1601-
611 12
612 22. Yokoyama C, Wang X, Briggs MR, Admon A, Wu J, Hua X*, et al.* SREBP-1, a basic-
613 helix-loop-helix-leucine zipper protein that controls transcription of the low density
614 lipoprotein receptor gene. Cell **1993**;75:187-97
615 23. Horton JD, Goldstein JL, Brown MS. SREBPs: activators of the complete program of
616 cholesterol and fatty acid synthesis in the liver. The Journal of clinical investigation
617 **2002**;109:1125-31
618 24. Moslehi A, Hamidi-Zad Z. Role of SREBPs in Liver Diseases: A Mini-review. J Clin
619 Transl Hepatol **2018**;6:332-8
620 25. Guo D, Bell EH, Mischel P, Chakravarti A. Targeting SREBP-1-driven lipid metabolism
621 to treat cancer. Current pharmaceutical design **2014**;20:2619-26
622 26. Deng Q, Li X, Fu S, Yin L, Zhang Y, Wang T*, et al.* SREBP-1c gene silencing can
623 decrease lipid deposits in bovine hepatocytes cultured in vitro. Cellular physiology and
624 biochemistry : international journal of experimental cellular physiology, biochemistry,
625 and pharmacology **2014**;33:1568-78
626 27. Li X, Li Y, Yang W, Xiao C, Fu S, Deng Q*, et al.* SREBP-1c overexpression induces

627 triglycerides accumulation through increasing lipid synthesis and decreasing lipid
628 oxidation and VLDL assembly in bovine hepatocytes. The Journal of steroid
629 biochemistry and molecular biology **2014**;143:174-82
630 28. Fang DL, Wan Y, Shen W, Cao J, Sun ZX, Yu HH*, et al.* Endoplasmic reticulum stress
631 leads to lipid accumulation through upregulation of SREBP-1c in normal hepatic and
632 hepatoma cells. Mol Cell Biochem **2013**;381:127-37
633 29. Ostermeyer AG, Paci JM, Zeng Y, Lublin DM, Munro S, Brown DA. Accumulation of
634 caveolin in the endoplasmic reticulum redirects the protein to lipid storage droplets. The
635 Journal of cell biology **2001**;152:1071-8
636 30. Mao X, Tey SK, Ko FCF, Kwong EML, Gao Y, Ng IO*, et al.* C-terminal truncated HBx
637 protein activates caveolin-1/LRP6/β-catenin/FRMD5 axis in promoting
638 hepatocarcinogenesis. Cancer letters **2019**;444:60-9
639 31. Schrader M, Costello J, Godinho LF, Islinger M. Peroxisome-mitochondria interplay and
640 disease. Journal of inherited metabolic disease **2015**;38:681-702
641 32. Sato A, Kawano H, Notsu T, Ohta M, Nakakuki M, Mizuguchi K*, et al.* Antiobesity
642 effect of eicosapentaenoic acid in high-fat/high-sucrose diet-induced obesity: importance
643 of hepatic lipogenesis. Diabetes **2010**;59:2495-504
644 33. Takeuchi Y, Yahagi N, Izumida Y, Nishi M, Kubota M, Teraoka Y*, et al.* Polyunsaturated
645 fatty acids selectively suppress sterol regulatory element-binding protein-1 through

proteolytic processing and autoloop regulatory circuit. The Journal of biological chemistry **2010**;285:11681-91

34. Tajima-Shirasaki N, Ishii K-A, Takayama H, Shirasaki T, Iwama H, Chikamoto K*, et al.* Eicosapentaenoic acid down-regulates expression of the selenoprotein P gene by inhibiting SREBP-1c protein independently of the AMP-activated protein kinase pathway in H4IIEC3 hepatocytes. The Journal of biological chemistry **2017**;292:10791-800

35. Ou J, Tu H, Shan B, Luk A, DeBose-Boyd RA, Bashmakov Y*, et al.* Unsaturated fatty acids inhibit transcription of the sterol regulatory element-binding protein-1c (SREBP-1c) gene by antagonizing ligand-dependent activation of the LXR. Proceedings of the National Academy of Sciences of the United States of America **2001**;98:6027-32

36. Wang C-C, Ding L, Zhang L-Y, Shi H-H, Xue C-H, Chi N-Q*, et al.* A pilot study on the effects of DHA/EPA-enriched phospholipids on aerobic and anaerobic exercises in mice. Food & Function **2020**;11:1441-54

37. Pinel A, Pitois E, Rigaudiere J-P, Jouve C, De Saint-Vincent S, Laillet B*, et al.* EPA prevents fat mass expansion and metabolic disturbances in mice fed with a Western diet. Journal of lipid research **2016**;57:1382-97

38. Oono K, Ohtake K, Watanabe C, Shiba S, Sekiya T, Kasono K. Contribution of Pyk2 pathway and reactive oxygen species (ROS) to the anti-cancer effects of

665 eicosapentaenoic acid (EPA) in PC3 prostate cancer cells. Lipids in Health and Disease
666 **2020**;19:15
667 39. deGraffenried LA, Friedrichs WE, Fulcher L, Fernandes G, Silva JM, Peralba JM*, et al.*
668 Eicosapentaenoic acid restores tamoxifen sensitivity in breast cancer cells with high Akt
669 activity. Annals of Oncology **2003**;14:1051-6

670

671

672 **Figure legends**

673 *Figure 1 ACADM underexpression correlated to worse prognosis in HCC.*

674 (A) ACADM was underexpressed in 64% of QMH clinical cases. (B) ACADM mRNA levels
675 were higher in non-tumour (NT) vs. tumour (T) cases, with TCGA data indicating lower
676 ACADM mRNA expression in tumours. (C) ACADM mRNA expression reduced with HCC
677 stage progression. The mRNA expression of HPRT, a housekeeping gene, was used for
678 normalisation. (D) ACADM underexpression correlated to various clinicopathological
679 parameters. (E) ACADM expression in tissue microarray samples. Intensity scores of ACADM
680 were generally high (scores 2 to 3) in non-tumourous tissues vs. the low scores (0 to 1) observed
681 in tumourous tissues. Scale bar, 100 μm. (F) Magnification of the HCC and the corresponding
682 NT tissue cores from two clinical cases to show the cell morphology and stain intensities of
683 ACADM. The pie chart depicted ACADM to be underexpressed (T < NT) in 86.3% of HCC

684 cases compared to 13.7% without underexpression. HPRT = Hypoxanthine-guanine
685 phosphoribosyltransferase.
686
687 *Figure 2 Suppression of ACADM diminishes β-oxidation and promotes HCC*
688 *tumourigenicity.*
689 (A) Western blot validated ACADM knockdown in Huh7 cells (sh61 and sh65) compared to
690 the stable non-target control. (B) Nile Red staining, triglyceride and phospholipid levels in cells.
691 Scale bar, 50 μm. (C) The fatty acid oxidation assay was used to determine the cellular
692 respiration rate of control and ACADM knockdown cells. (D) Fatty acid profiling of Huh7 cells
693 detected the total fatty acids, different fatty acid chain lengths and types found in shACADM
694 cells. (E) MTT assay, soft agar (scale bar, 90 μm), migration and invasion assays (scale bar,
695 200 μm) were used to indicate the aggressiveness of HCC cells upon ACADM knockdown. (F)
696 In subcutaneous xenografts of Huh7 cells injected into nude mice (n = 6), the tumour volume
697 and weight of tumours were measured. (G) Immunohistochemical staining of shCTL and
698 shACADM in subcutaneous xenografts was performed. Quantification of ACADM and Ki67
699 signal are shown. (H) Hydrodynamic injection was performed in mice (n = 12), split into three
700 groups for injection of different plasmid combinations to compare their effects. Number of
701 tumour nodules was counted and nodule size was measured. (I) Representative images showing
702 immunohistochemical staining of ACADM, N-Ras and p53 of the excised livers of mice at the

703 end of the experiment. Arrows indicate lymphoid cells as positive control for p53 staining
704 which was not detected in tumour cells. Scale bar, 50 μm.
705
706 *Figure 3 SREBP-1 is the direct upstream negative transcriptional regulator of ACADM*
707 *along the Cav1/SREBP-1/ACADM axis.*
708 (A) Schematic diagram to show the mutation of the PPRE and SRE binding sites in the full-
709 length (-1450) ACADM promoter (*left*). ACADM promoter activity was significantly
710 upregulated upon mutation of the SRE but not the PPRE site (*middle*). ChIP assay revealed the
711 enrichment of ACADM promoter fragments in the presence of SREBP-1 compared to IgG
712 control. ACADM-540F and ACADM+41R primers are flanking the SREBP-1 binding site
713 (SRE) and ACADM-1450-F and ACADM-950-R primers are flanking the unrelated promoter
714 region (*right*). (B) Correlation between SREBP-1 and ACDAM expression in paired cases of
715 tumour (T) and non-tumourous tissues (NT). Representative cases with and without SREBP-1
716 and the corresponding ACADM expression are shown. The signal intensities of SREBP-1 and
717 ACADM expressions are quantified and the IHC H-scores are shown. Scale bar, 100 μm. (C)
718 SREBP-1 expression in tissue microarray samples. Intensity scores of SREBP-1 were generally
719 low (scores 0 to 1) in non-tumourous tissues vs. the higher scores (2 to 3) observed in
720 tumourous tissues. The H-scores indicated the extent of nuclear immunoreactivity of SREBP-
721 1 in tissues. Magnification of the HCC and the corresponding NT tissue cores from two clinical

722 cases to show the cell morphology and stain intensities of SREBP-1. The pie chart depicted
723 SREBP-1 to be overexpressed (T > NT) in 56.5% of HCC cases compared to 43.5% without
724 overexpression. (D) ACADM promoter activity was upregulated in MHCC97L shCav1 cells
725 compared to shCTL cells. (E) Cellular fractionation of MHCC97L shCTL and shCav1 cells,
726 and of MHCC97L cells with or without filipin treatment, was performed and analysed for the
727 indicated protein expressions by western blotting. (F) Western blot analysis of ACADM
728 expression in MHCC97L shCav1 cells stably expressing SREBP-1. (G) The ACADM
729 expression in MHCC97L cells transiently transfected with siRNA targeting SREBP-1 was
730 examined by immunoblotting.
731
732 *Figure 4 Cav1 promotes HCC via regulating lipid metabolism.*
733 (A) Western blot revealed Cav1 expression in MHCC97L stable non-target control (shCTL)
734 and Cav1 knockdown clones (shCav1#1 and #2). (B) The cellular triglycerides (Tg),
735 phospholipids and Nile Red staining of the oil droplets in cells. DAPI was used to stain the
736 nuclei blue. The Nile Red signal intensity was quantified using ImageJ software (NIH). Scale
737 bar, 50 μm. (C) The fatty acid oxidation assay was used to determine the cellular respiration
738 rate of HCC cells. (D) The addition of ETO restored the triglycerides, phospholipids and
739 cellular lipids (scale bar, 50 μm) of shCav1 cells, with their promoted cell aggressiveness as
740 demonstrated by the (E) cell proliferation rate, anchorage independent growth (scale bar, 90

μm), migration and invasiveness (scale bar, 200 μm). (F) Subcutaneous xenografts from nude mice injected intraperitoneally with ETO significantly increased the volume and weight of tumours derived from shCav1 MHCC97L cells. ETO was injected twice a week for four weeks before tumour harvest. Immunohistochemistry revealed the increased levels of Cav1 and oil droplets in the xenografts from mice injected with ETO compared to the ones without. (G) The fatty acid oxidation assay was performed using MHCC97L shCav1 cells overexpressing SREBP-1. (H) MHCC97L shCav1 cells with SREBP-1 overexpression was subjected to colony formation, migration and invasion assays.

Figure 5 *Negative correlation between Cav1 and ACADM expressions.*

(A) RT-qPCR and (B) western blot revealed the inversely correlated ACADM and Cav1 mRNA and protein levels in the HCC cell line panel, respectively. Cells were ordered in increasing aggressiveness from left to right. (C) Immunohistochemical staining of Cav1 and ACADM in the MHCC97L subcutaneous xenografts. Scale bar, 50 μm. (D) RT-qPCR and (E) western blot indicated the mRNA and protein levels of ACADM in Hep3B and MHCC97L shCav1 cells. (F) TCGA and in-house clinical data revealed their inversed mRNA correlation.

Figure 6 *Suppression of ACADM results in accumulation of fatty acids and aggressiveness of Cav1 knockdown cells.*

760 (A) Western blot revealed the expression of ACADM after ACADM knockdown in MHCC97L
761 and Hep3B shCav1 cells (shCav1/sh61 and shCav1/sh65). (B) Cellular triglyceride and
762 phospholipid levels, and (C) Nile Red staining of the lipid droplets in cells. Scale bar, 50 μm.
763 (D) Fatty acid oxidation assay was performed using MHCC97L and Hep3B cells with double
764 knockdown of Cav1 and ACADM. The (E) soft agar (scale bar, 90 μm), (F) migration and (G)
765 invasion assays (scale bar, 200 μm) defined the aggressiveness of HCC cells upon ACADM
766 knockdown in shCav1 cells. (H) Subcutaneous xenografts of MHCC97L shCTL, shCav1 and
767 shCav1/sh61 cells in nude mice (n = 6). Tumours dissected from mice at the end of the
768 experiment are shown. Tumour weight and volume are measured. (I) Immunohistochemical
769 staining of Cav1, ACADM, CD31 and Ki67 in xenograft tissues. The quantification of Ki67
770 positive signal is shown. Scale bar, 50 μm.
771
772 *Figure 7 Inhibition of SREBP-1 enhanced sorafenib efficacy in vivo.*
773 (A) Western blot analysis of SREBP-1 expression in MHCC97L cells treated with vehicle or
774 EPA. (B) Oral gavage feeding chart of drugs into mice over a period of 21 days. (C) The tumour
775 size was measured daily and the tumour volume was calculated and plotted. (D) Image of
776 excised subcutaneous xenografts, with the tumour volume and weight of the tumours measured
777 and plotted. (E) Immunohistochemical staining indicated the expressions of SREBP-1,
778 ACADM and Ki67 in the excised subcutaneous tumours. Cells with positive Ki67 expression

779 and nuclear stain of SREBP-1 were quantified. Scale bar, 50 μm. (F) Visual summary of the
780 findings in this study. In normal liver cells, SREBP-1 accumulates in the nucleus to modulate
781 ACADM transcription, resulting in the regulation of β-oxidation to breakdown fatty acids. In
782 HCC cells, increased Cav1 enhanced the nuclear accumulation of SREBP-1, which suppressed
783 ACADM transcription, leading to decreased β-oxidation and the accumulation of fatty acids,
784 contributing to the augmented tumour growth, migration and invasiveness of cancer cells; EPA
785 administration abrogated these effects.

Figure 1

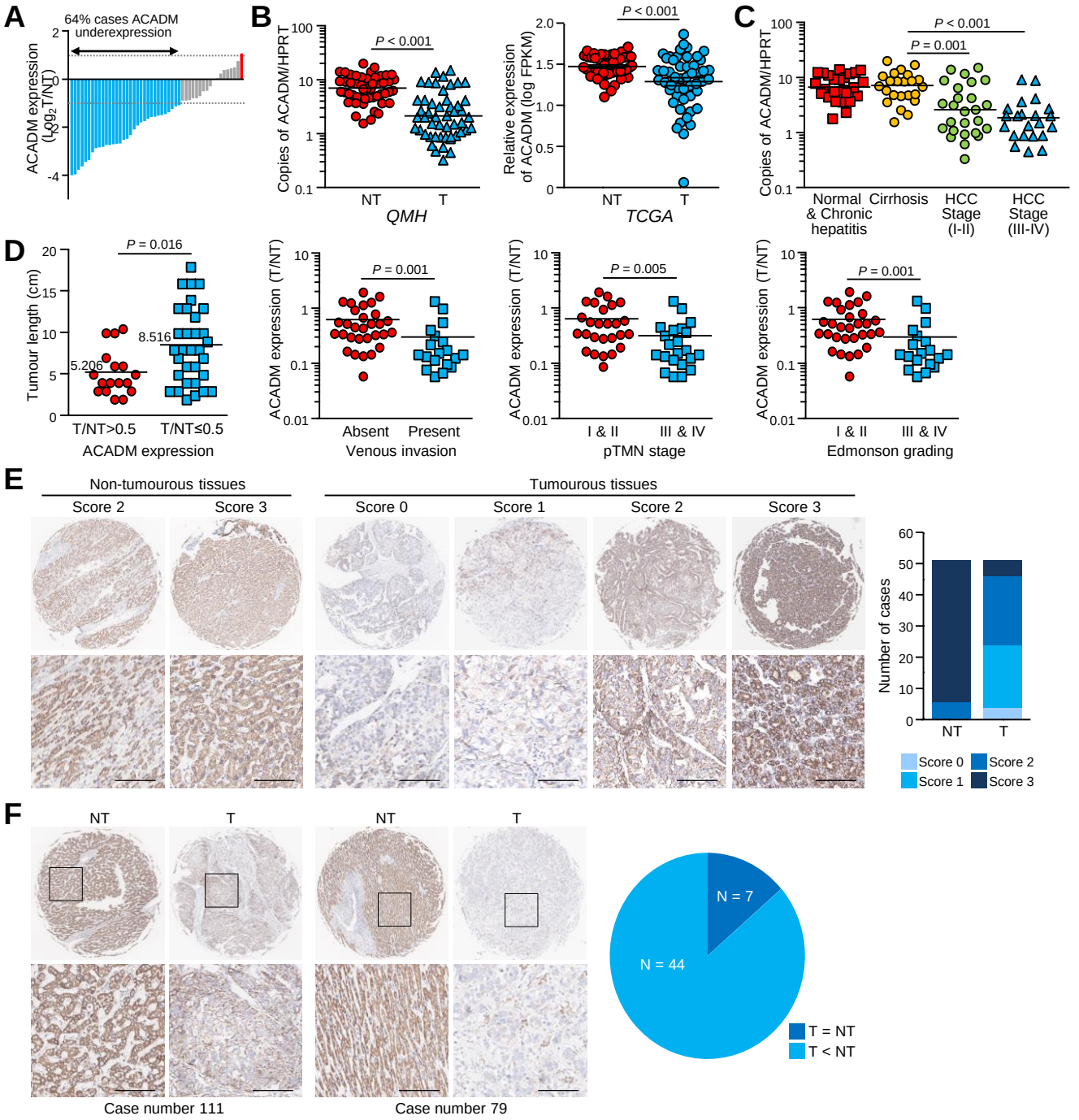
A
64% cases ACADM underexpression
ACADM expression (Log2 T/NT)
B
Copies of ACADM/HPRT
P < 0.001
NT
T
QMH
Relative expression of ACADM (log FPKM)
P < 0.001
TCGA
C
Copies of ACADM/HPRT
P < 0.001
P = 0.001
Normal & Chronic hepatitis
Cirrhosis
HCC Stage (I-II)
HCC Stage (III-IV)
D
Tumour length (cm)
P = 0.016
5.206
8.516
T/NT>0.5
T/NT≤0.5
ACADM expression
ACADM expression (T/NT)
P = 0.001
Absent
Present
Venous invasion
P = 0.005
I & II
III & IV
pTMN stage
P = 0.001
Edmonson grading
E
Non-tumourous tissues
Score 2
Score 3
Tumourous tissues
Score 0
Score 1
Score 2
Score 3
Number of cases
NT
T
Score 0
Score 1
Score 2
Score 3
F
NT
T
NT
T
Case number 111
Case number 79
N = 7
N = 44
T = NT
T < NT

Figure 2

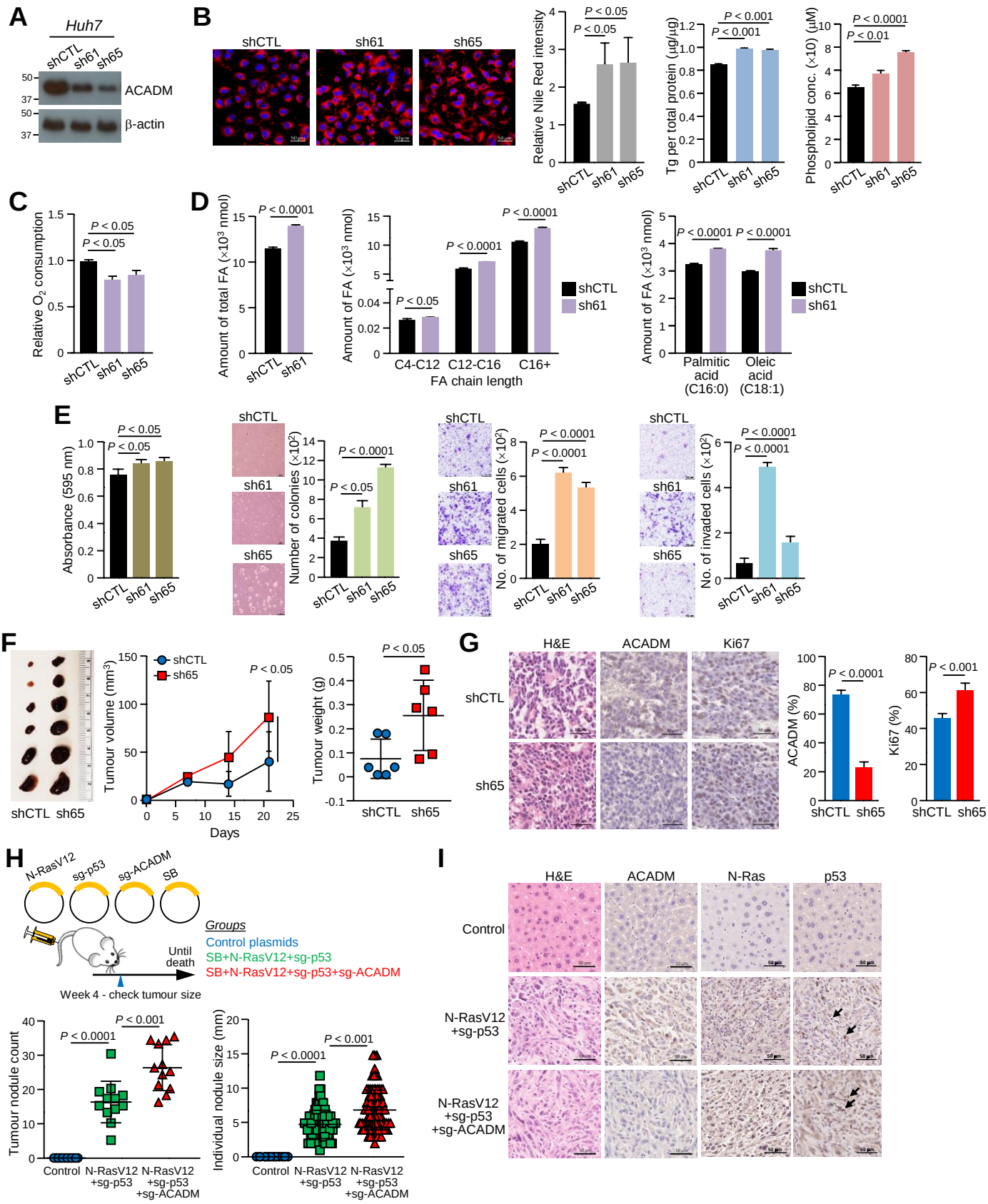
A
Huh7
shCTL
sh61
sh65
50
37
ACADM
β-actin
B
shCTL
sh61
sh65
Relative Nile Red intensity
Tg per total protein (μg/μg)
Phospholipid conc. (×10) (μM)
P < 0.05
P < 0.001
P < 0.0001
P < 0.01
C
Relative O2 consumption
D
Amount of total FA (×10³ nmol)
Amount of FA (×10³ nmol)
C4-C12
C12-C16
C16+
FA chain length
Palmitic acid (C16:0)
Oleic acid (C18:1)
E
Absorbance (595 nm)
Number of colonies (×10²)
No. of migrated cells (×10²)
No. of invaded cells (×10²)
F
Tumour volume (mm³)
Days
Tumour weight (g)
G
H&E
ACADM
Ki67
ACADM (%)
Ki67 (%)
H
N-RasV12
sg-p53
sg-ACADM
SB
Until death
Week 4 - check tumour size
Groups
Control plasmids
SB+N-RasV12+sg-p53
SB+N-RasV12+sg-p53+sg-ACADM
Tumour nodule count
Individual nodule size (mm)
Control
N-RasV12 +sg-p53
N-RasV12 +sg-p53 +sg-ACADM
I
H&E
ACADM
N-Ras
p53
Control
N-RasV12 +sg-p53
N-RasV12 +sg-p53 +sg-ACADM

Figure 3

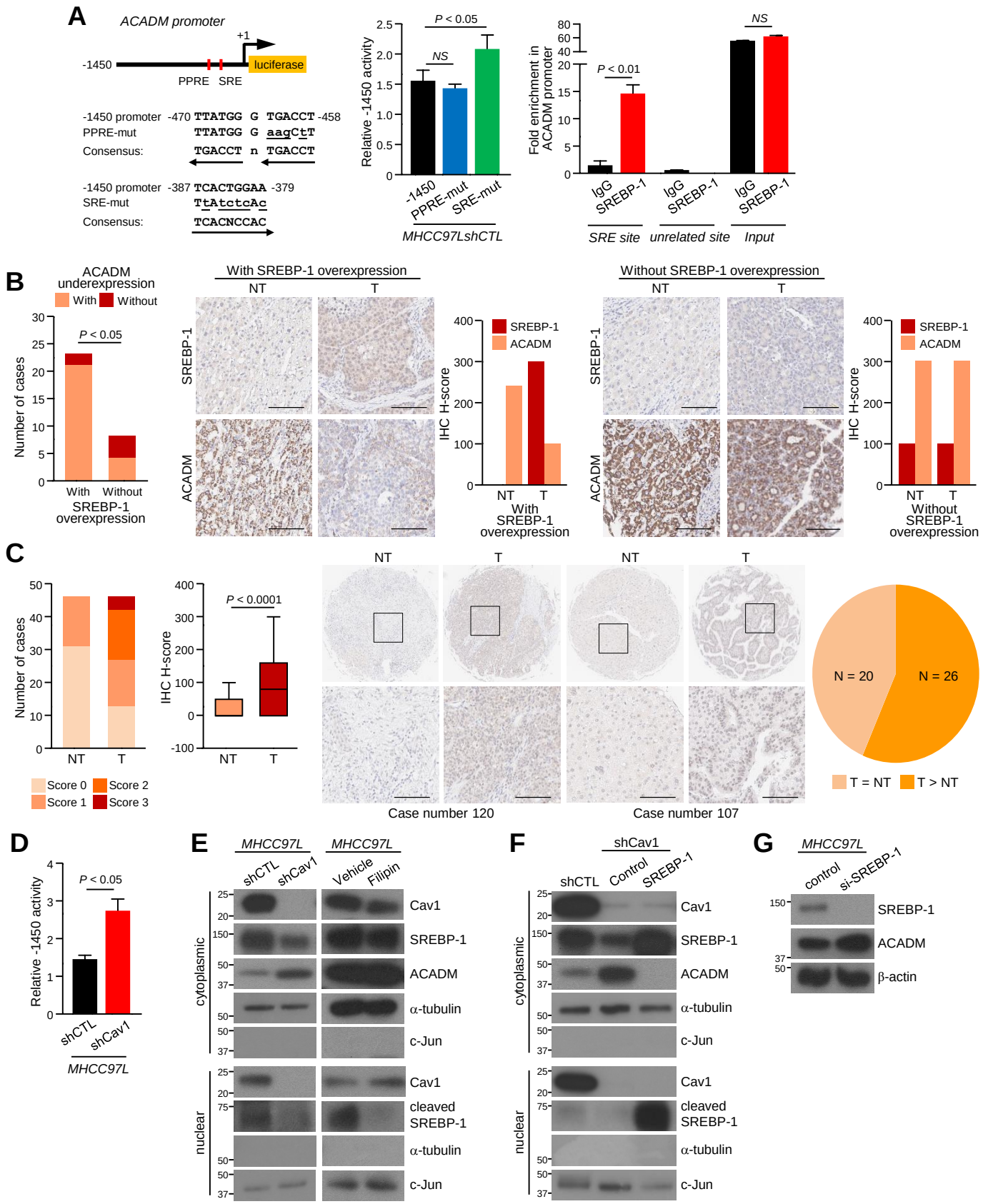
A
ACADM promoter
+1
-1450
luciferase
PPRE SRE
-1450 promoter -470 TTATGG G TGACCT -458
PPRE-mut TTATGG G aagCtT
Consensus: TGACCT n TGACCT
-1450 promoter -387 TCACTGGAA -379
SRE-mut TtAtctcAc
Consensus: TCACNCCAC
Relative -1450 activity
P < 0.05
NS
-1450
PPRE-mut
SRE-mut
MHCC97LshCTL
Fold enrichment in ACADM promoter
P < 0.01
NS
IgG
SREBP-1
SRE site
unrelated site
Input
B
ACADM underexpression
With
Without
P < 0.05
Number of cases
SREBP-1 overexpression
With SREBP-1 overexpression
Without SREBP-1 overexpression
NT
T
SREBP-1
ACADM
IHC H-score
C
Score 0
Score 1
Score 2
Score 3
P < 0.0001
Case number 120
Case number 107
N = 20
N = 26
T = NT
T > NT
D
P < 0.05
Relative -1450 activity
shCTL
shCav1
MHCC97L
E
MHCC97L
Vehicle
Filipin
cytoplasmic
nuclear
Cav1
SREBP-1
ACADM
α-tubulin
c-Jun
cleaved SREBP-1
F
shCav1
Control
SREBP-1
G
control
si-SREBP-1
β-actin

Figure 4

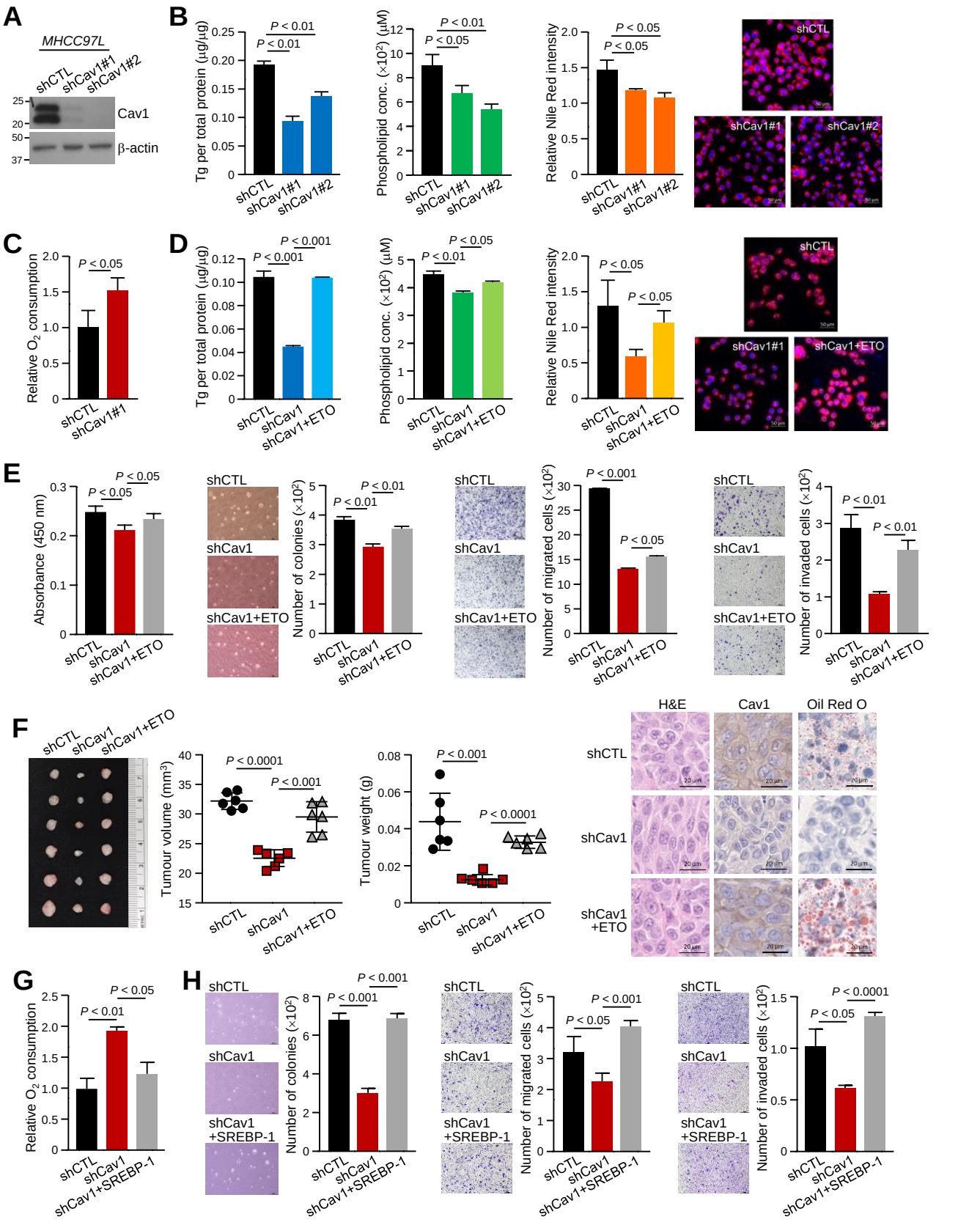
A
MHCC97L
shCTL
shCav1#1
shCav1#2
Cav1
β-actin
B
Tg per total protein (μg/μg)
Phospholipid conc. (×10²) (μM)
Relative Nile Red intensity
C
Relative O2 consumption
D
E
Absorbance (450 nm)
Number of colonies (×10²)
Number of migrated cells (×10²)
Number of invaded cells (×10²)
F
Tumour volume (mm³)
Tumour weight (g)
H&E
Cav1
Oil Red O
shCav1+ETO
G
shCav1+SREBP-1
H

Figure 5

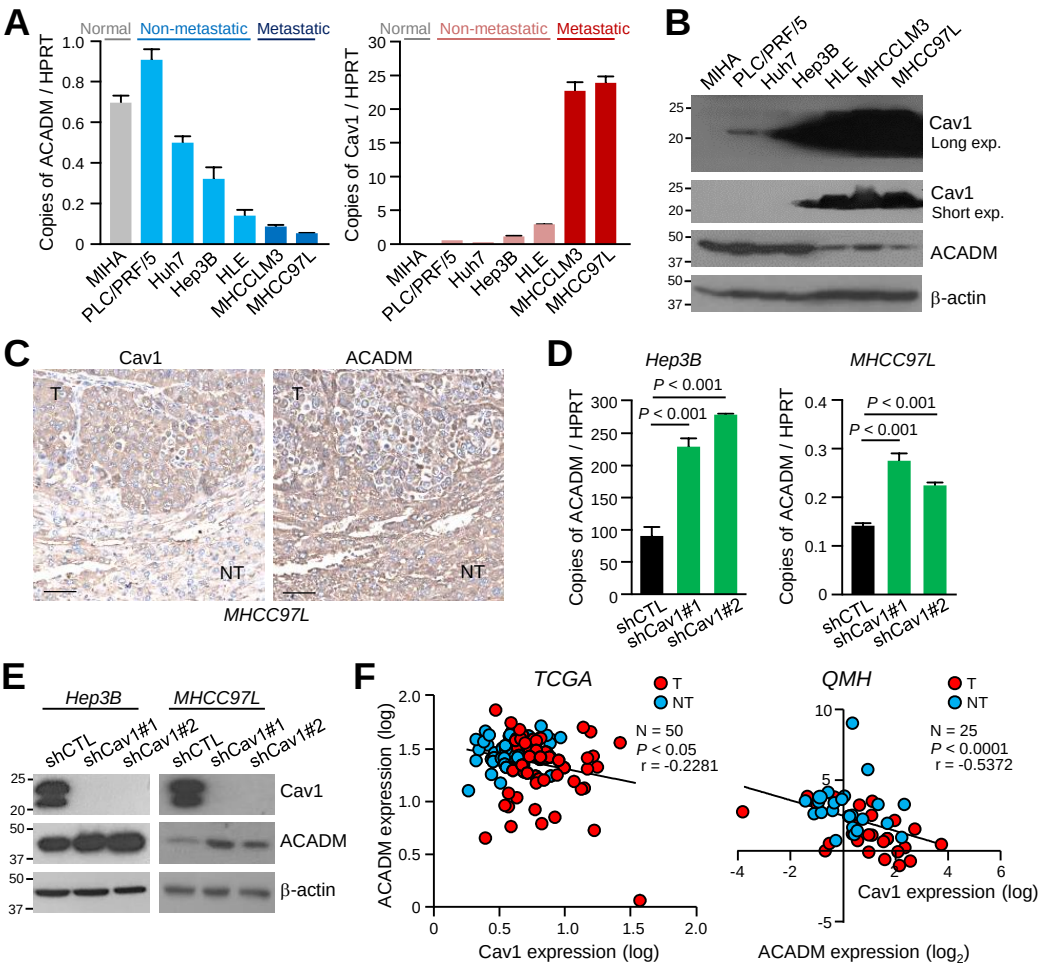
A
Normal
Non-metastatic
Metastatic
Copies of ACADM / HPRT
Copies of Cav1 / HPRT
MIHA
PLC/PRF/5
Huh7
Hep3B
HLE
MHCCLM3
MHCC97L
B
Cav1
Long exp.
Cav1
Short exp.
ACADM
β-actin
C
Cav1
ACADM
T
NT
MHCC97L
D
Hep3B
MHCC97L
P < 0.001
Copies of ACADM / HPRT
shCTL
shCav1#1
shCav1#2
E
Hep3B
MHCC97L
shCTL
shCav1#1
shCav1#2
Cav1
ACADM
β-actin
F
TCGA
QMH
T
NT
N = 50
P < 0.05
r = -0.2281
N = 25
P < 0.0001
r = -0.5372
ACADM expression (log)
Cav1 expression (log)
ACADM expression (log2)

Figure 6

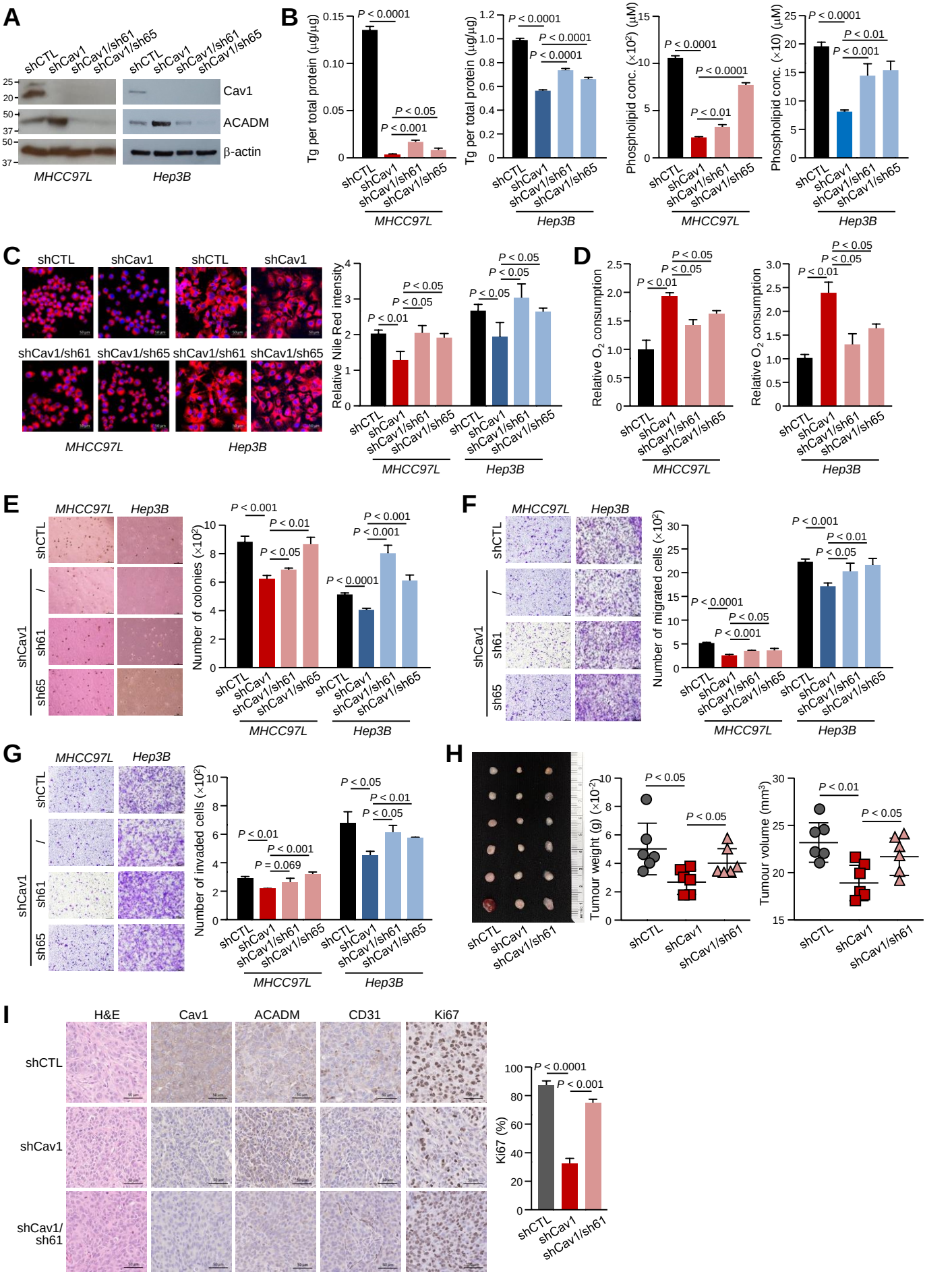
A
shCTL
shCav1
shCav1/sh61
shCav1/sh65
Cav1
ACADM
β-actin
MHCC97L
Hep3B
B
Tg per total protein (μg/μg)
Phospholipid conc. (×10²) (μM)
Phospholipid conc. (×10) (μM)
C
Relative Nile Red intensity
D
Relative O2 consumption
E
Number of colonies (×10²)
F
Number of migrated cells (×10²)
G
Number of invaded cells (×10²)
H
Tumour weight (g) (×10⁻²)
Tumour volume (mm³)
I
H&E
Cav1
ACADM
CD31
Ki67
Ki67 (%)

Figure 7

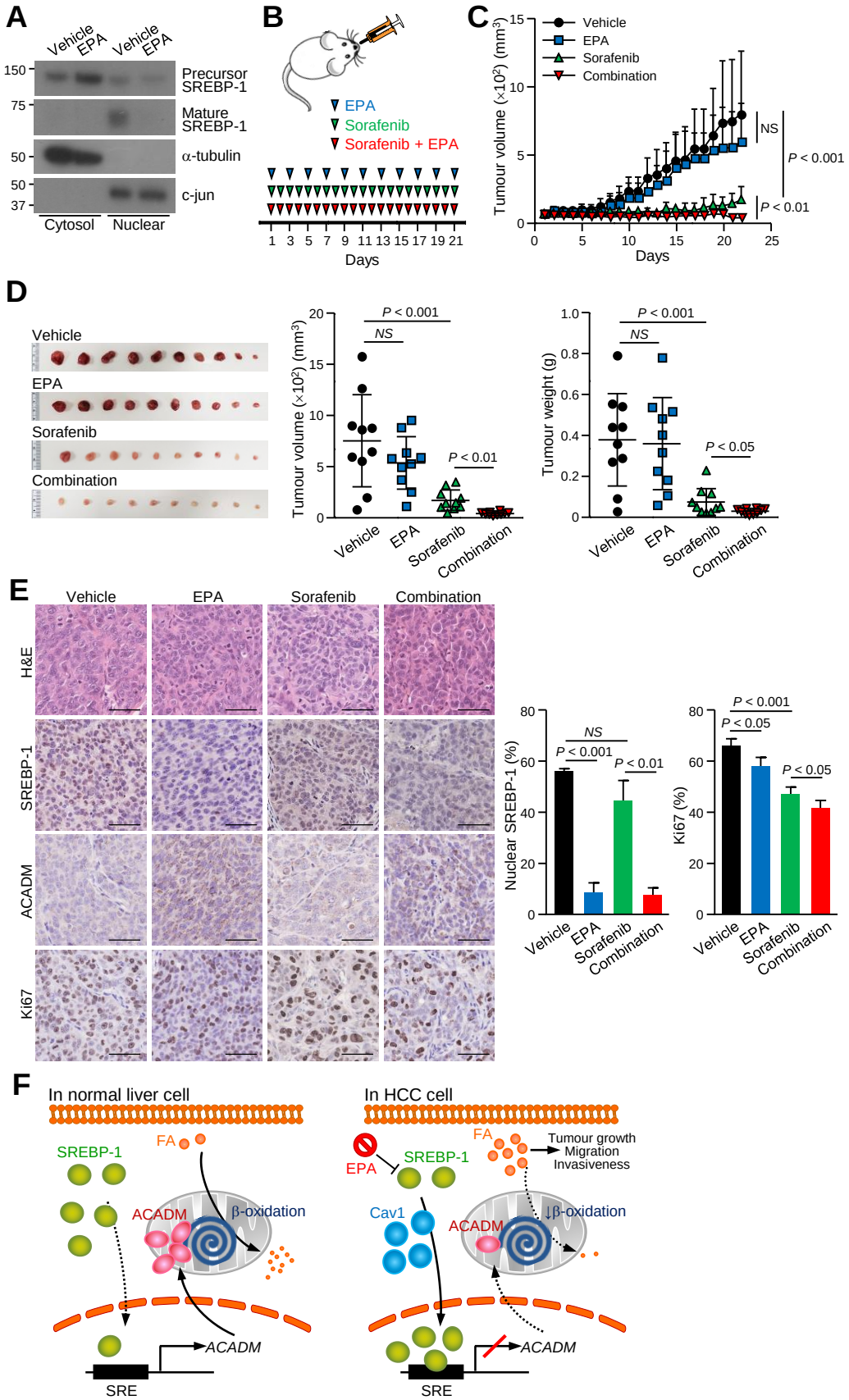
A
Vehicle
EPA
Vehicle
EPA
150
75
50
50
37
Precursor SREBP-1
Mature SREBP-1
α-tubulin
c-jun
Cytosol
Nuclear
B
EPA
Sorafenib
Sorafenib + EPA
1 3 5 7 9 11 13 15 17 19 21
Days
C
Vehicle
EPA
Sorafenib
Combination
Tumour volume (×10²) (mm³)
NS
P < 0.001
P < 0.01
Days
D
Vehicle
EPA
Sorafenib
Combination
Tumour volume (×10²) (mm³)
P < 0.001
NS
P < 0.01
Tumour weight (g)
P < 0.001
NS
P < 0.05
E
Vehicle
EPA
Sorafenib
Combination
H&E
SREBP-1
ACADM
Ki67
Nuclear SREBP-1 (%)
NS
P < 0.001
P < 0.01
Ki67 (%)
P < 0.001
P < 0.05
P < 0.05
F
In normal liver cell
SREBP-1
FA
ACADM
β-oxidation
ACADM
SRE
In HCC cell
EPA
SREBP-1
FA
Tumour growth
Migration
Invasiveness
Cav1
ACADM
↓β-oxidation
ACADM
SRE

Suppression of ACADM-mediated fatty acid oxidation promotes hepatocellular carcinoma via aberrant Cav1/SREBP-1 signaling

Angel P. Y. Ma[1], Cherlie L. S. Yeung[1], Sze Keong Tey[1], Xiaowen Mao[1], Samuel W. K. Wong[1], Tung Him Ng[1], Frankie C. F. Ko[1], Ernest M. L. Kwong[1], Alexander H. N. Tang[1], Irene Oi-Lin Ng[1,2], Shao Hang Cai[3], Jing Ping Yun[4], Judy W. P. Yam[1,2]

Supplementary Materials and methods

Supplementary Figures

Supplementary Tables

Supplementary Materials and methods

Protein extraction and western blotting

To collect cell pellets for protein extraction, sub-confluent cells were collected and then washed with ice-cold PBS to remove residual culture medium. The cells were lysed using RIPA lysis buffer on ice for 30 minutes before centrifugation to obtain the cell lysate in the supernatant, which was kept on ice after extraction. The NE-PER^{TM} Nuclear and Cytoplasmic Extraction Reagents (Thermo Scientific) were used to separate cytoplasmic and nuclear extracts from cells. The extraction was carried out according to the manufacturer's protocol.

The Bradford reagent (Bio-Rad Laboratories) was used to determine the concentration of the cell lysate according to the manufacturer's instructions. Concentration determination were done in triplicates per sample. Absorbance reading was measured at 595 nm by the Infinite® F200 microplate reader (Tecan, Switzerland).

For protein detection, 30 μg of protein lysate per sample were used. Proteins were separated by sodium dodecyl sulfate-polyacrylamide gel electrophoresis (SDS-PAGE) and transferred to the 0.45 μM polyvinylidene difluoride blotting membrane (Amersham™ Hybond™, GE Healthcare). The membranes were blocked with 5% semi-skimmed milk in 1× TBST at room

temperature for 1 hour, then incubated with primary antibodies against Cav1 (BD Biosciences Cat# 610406, RRID:AB_397788), ACADM (Abcam Cat# ab92461, RRID:AB_10563530), SREBP-1 (Santa Cruz Biotechnology Cat# sc-13551, RRID:AB_628282), β-actin (Sigma-Aldrich Cat# A5316, RRID:AB_476743), α-tubulin (Sigma-Aldrich Cat# T9026, RRID:AB_477593) and c-Jun (BD Biosciences Cat# 610326, RRID:AB_397716) overnight at 4°C. The proteins were detected with the ECL™ western blotting detection system (Amersham™ GE Healthcare) according to the manufacturer's instructions.

Co-immunoprecipitation (Co-IP)

CoIP was performed to investigate the putative interaction between Cav1 and SREBP-1. In brief, cell lysates to be analysed were collected with NETN lysis buffer. Proteins were incubated with primary antibody and subsequently with 50% Protein G beads (GE). The protein-beads were then pelleted, washed and resuspended in 2× SDS loading dye, then boiled at 95°C for 5 minutes before being subjected to SDS-PAGE followed by western blot analysis.

Dual luciferase reporter assay

The full-length DNA encoding for the ACADM promoter was amplified by PCR using primers, ACADM-1450-Kpn-F and ACADM+41-Bgl-R (Supplementary Table 2). The PCR products were purified and cloned into the pGL3-Basic vector (Promega). pGL3-Basic vector carrying

ACADM promoter together with Renilla luciferase were transfected into cells using Lipofectamine® 2000 reagent (Invitrogen). For the detection of ACADM promoter activity, the Dual-Luciferase® reporter assay system (Promega) was employed according to the manufacturer's instructions. Readings were taken using the Infinite® F200 microplate reader (Tecan).

Detection of mRNA with Quantitative real-time polymerase chain reaction

Trizol® Reagent (Invitrogen) was used for RNA extraction from cells according to the manufacturer's protocol. Concentration and quality of the resulting RNA were determined using BioDrop µLITE (BioDrop, United Kingdom). For reverse transcription of RNA to cDNA, 1 µg of RNA was added to 4 µl of SuperScript® VILO™ Master mix (Invitrogen) in a total volume of 20 µl and subjected to PCR cycle conditions of 25°C for 10 minutes, 42°C for 1 hour and 85°C for 5 minutes.

Quantitative PCR was performed on the ABI7900HT Fast Real Time PCR system (Applied Biosystems), with each sample assayed in triplicates on a 96-well reaction plate. The reactions were carried out with the following TaqMan probes (ThermoFisher Scientific): Cav1, ACADM, ACADL, ACADS and ECHDC3. The relative expression was normalised with the housekeeping gene hypoxanthine guanine phosphoribosyltransferase (HPRT) (Applied

Biosystems).

Immunohistochemistry (IHC)

Prior to paraffin embedding, human or mouse tissues were fixed with 10% formaldehyde and washed with 70% ethanol. The paraffin block was then sectioned into 5 μm sections for IHC staining. Paraffin sections were dewaxed with xylene, then rehydrated in a decreasing alcohol concentration gradient before rinsing with water. Antigens were retrieved in antigen retrieval buffer by boiling for 5 minutes. Slides were allowed to cool at room temperature before rinsing in water. To block any endogenous peroxidase activity, slides were incubated in 10% hydrogen peroxidase solution in TBS for 20 minutes, followed by a 30 minutes incubation of 10% goat/mouse/rabbit serum. Sections were stained with primary antibodies overnight at 4°C, then incubated with horseradish peroxidase conjugated secondary antibodies for 30 minutes at room temperature. For histological analysis, dewaxed sections were counterstained with haematoxylin and eosin for several minutes. Histological analysis was carried out by pathologists and scanning of the slides was performed with Aperio ScanScope CS System camera to create high-quality digital slides for analysis.

Fatty acid oxidation assay

The Fatty Acid Oxidation Complete Assay Kit (Abcam) was used to detect the respiration rate

of cells according to the manufacturer's protocol. Briefly, cells were plated in triplicates in a 96-well plate, then incubated overnight at 37°C. The culture media was replaced with Glucose-Deprivation media and incubated for a further 24 hours. Reagents to be used were prepared freshly according to the manufacturer's protocol. Cells were washed twice with FA-free Measurement Media before the addition of FA/FA-free Measurement Media and O_2 consumption reagent. Controls were then added (ETO, FCCP or BSA). High Sensitivity mineral oil was used to seal the wells before fluorescence measurements were recorded with the Infinite® F200 microplate reader (Tecan, Switzerland). Kinetic data output was analysed to determine the FAO-driven electron transport chain activity.

Targeted metabolite relative quantification of fatty acids

Sample processing and gas chromatography-mass spectrometry (GC-MS) analysis were performed at the Proteomics and Metabolomics Core Facility, Li Ka Shing Faculty of Medicine, HKU. For Folch extraction, 100 µl of 200 ppm C19:0 fatty acid internal standard (Sigma-Aldrich) was spiked to ~10^7 cells. A modified Folch extraction procedure wherein 4.9 ml Chloroform/Methanol (2:1, v/v) was added to the cells. The mixture was subjected to 10 pulses of sonication before being centrifuged at 4,000 rpm for 5 minutes. The clear supernatant was added to NaCl/Water (0.73%, w/v), then vortexed for 30 seconds. The aqueous layer was discarded and the organic layer was washed twice using Methanol/Water (1:1, v/v) without

mixing, with the resulting organic layer evaporated under a gentle stream of nitrogen at 45°C. For esterification, the dried sample was dissolved in 0.1 ml of chloroform, 1 ml of methanol, and 50 µl of concentrated hydrochloric acid (35%, w/w). The solution was overlaid with nitrogen, vortexed, then heated at 100°C for 1 hour. Once cooled to room temperature, 1 ml of hexane (Acros) and 1 ml of water were added for fatty acid methyl ester extraction. After vortexing and phase separation, up to 1 µl of the hexane phase was injected for GC-MS analysis.

GC/MS chromatogram was acquired in SCAN and SIM mode in an Agilent 7890B GC - Agilent 7010 Triple Quadrapole Mass Spectrometer system. The sample was separated through an Agilent DB-23 capillary column (60 m × 0.25 mm ID, 0.15 µm film thickness) under constant pressure at 33.4 psi. Characteristic fragment ions (m/z 55, 67, 69, 74, 79, 81, 83, 87, 91, 93, 95, 96, 97, 115, 127, 143) were monitored in SIM mode throughout the run. Mass spectra from m/z 50-350 were acquired in SCAN mode. Data analysis was performed using the Agilent MassHunter Workstation Quantitative Analysis Software. Linear calibration curves for each analyte were generated by plotting peak area ratio of external/internal standard against standard concentration at different concentration level. Analytes were confirmed by comparing the ratio of characteristic fragment ions in the sample and standard.

Cell migration and invasion assays

To reproduce the ability of cells to migrate and invade into the vasculature from the tumour origin, cell migration and invasion assays were performed in triplicates using Transwell® migration chambers (Corning Costar). Optimal cell numbers specific for each cell line were resuspended in serum free medium before seeding into migration chambers; the full-medium in the bottom of the well creates a nutrient gradient which attract the cells in the chamber to migrate through the membrane. To assess the invasion ability of cells, an additional thin layer of 1× Matrigel™ membrane matrix (Corning) was coated onto the inner membrane of the chamber 30 minutes prior to cell seeding. After cell seeding into the chambers, the cells were allowed to migrate for 18 hours at 37°C. After incubation, the migrated and invaded cells were fixed in methanol and stained with 1× crystal violet. Four images of each chamber were visualised and photographed at random under a microscope fitted with a CCD camera (Nikon).

Soft agar assay

The soft agar assay was used to monitor the anchorage-independent growth ability of cells, and it comprises of single cells suspended in a layer of 0.4% agarose on top of a 1% agarose base. The plates were then wrapped in Parafilm and incubated at 37°C for 3-4 weeks to allow cell colonies to form. Each sample were assayed in triplicates. Twenty images of each plate were visualised and photographed at random under a microscope fitted with a CCD camera (Nikon).

MTT assay

To assess the proliferation rate of adherent cells, cells were seeded at a density of 2 x 10^3 cells per well of a 96-well plate in triplicate and cultured in full-DMEM for 24 hours. MTT labelling reagent was then added to a final concentration of 0.5 mg/ml per well before incubating the cells at 37°C for 4 hours. The labelling reagent was removed and 70 µl of DMSO solubilisation solution was added to each well before incubating for a further 15 minutes at room temperature. The resulting absorbance per well was measured at 595 nm with the Infinite® F200 microplate reader (Tecan).

Supplementary Figures

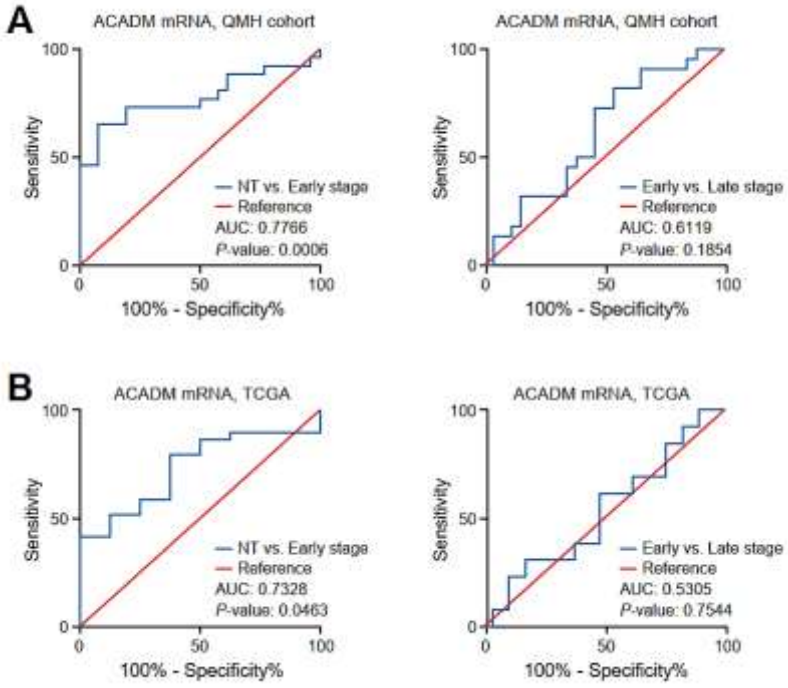

Supplementary Figure 1. ACADM expression is significantly related to the early stages of HCC. The receiver operating characteristic curves illustrated the significance of ACADM expression in relations to (A) the NT vs. early stage and early vs. late stage HCC in the QM cohort, with similar trends observed between ACADM and (B) early stage and late stage HCC data obtained from TCGA.

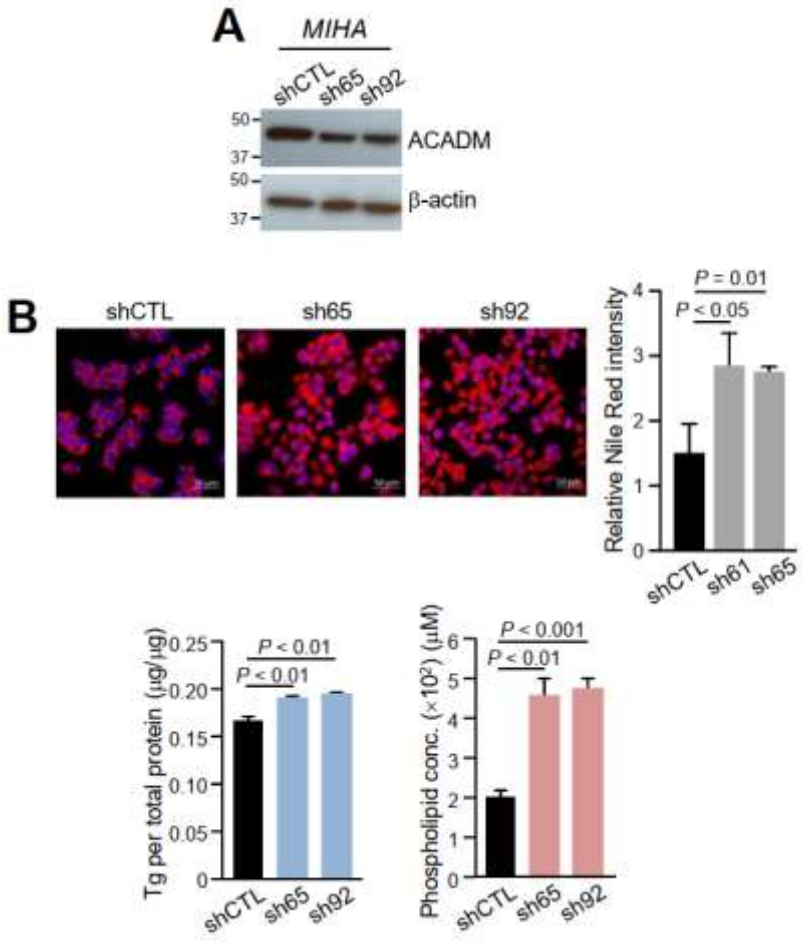

Supplementary Figure 2. Suppression of ACADM diminishes beta-oxidation.

(A) Western blot validated the knockdown efficiency of ACADM in MIHA knockdown clones (sh65 and sh92) compared to the stable non-target control (shCTL). (B) Nile Red staining (scale bar, 50 μm), triglyceride and phospholipid levels in cells.

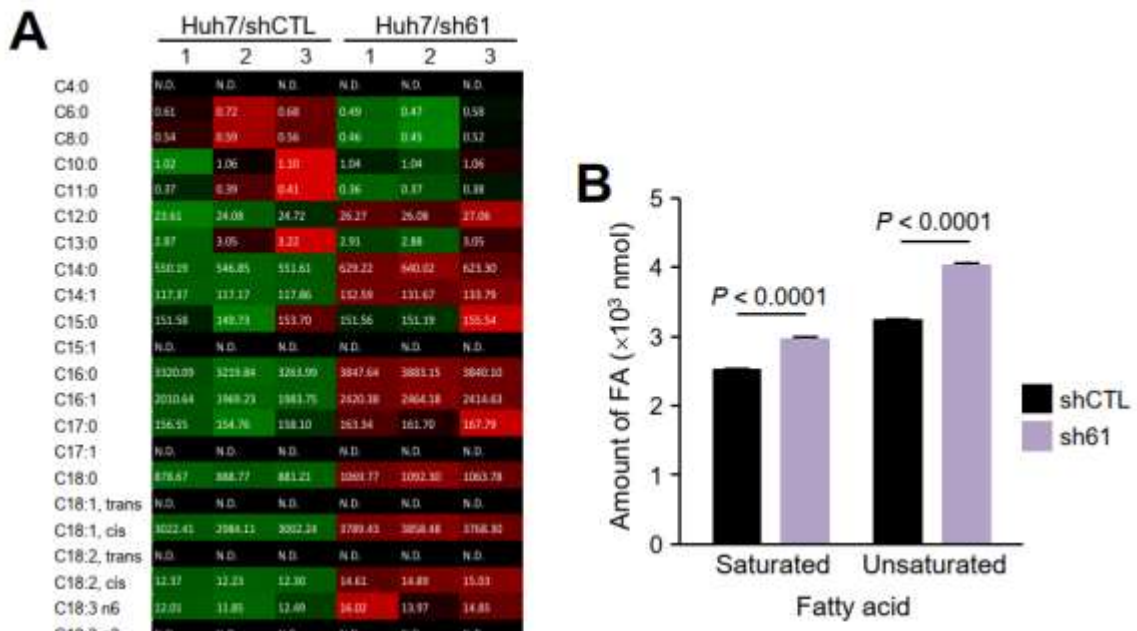

Supplementary Figure 3. Increased abundance of both saturated and unsaturated fatty acids in ACADM knockdown cells.

(A) Heat map and (B) bar chart illustrating the abundance of both saturated and unsaturated fatty acids in shACADM Huh7 cells compared to the shCTL. Green = low abundance and red = high abundance.

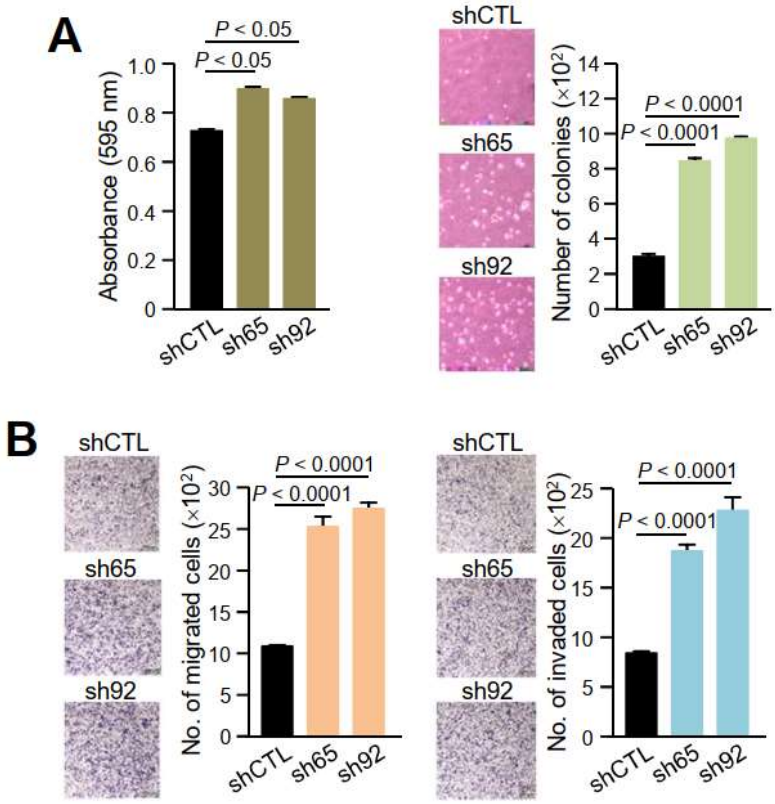

Supplementary Figure 4. Suppression of ACADM promotes proliferation, anchorage-independent growth, migration and invasion of immortalised normal liver cells.

The MTT, soft agar (scale bar, 90 μm) (A), migration and invasion assays (B) (scale bar, 200 μm) were used to indicate the aggressiveness of HCC cells upon ACADM knockdown.

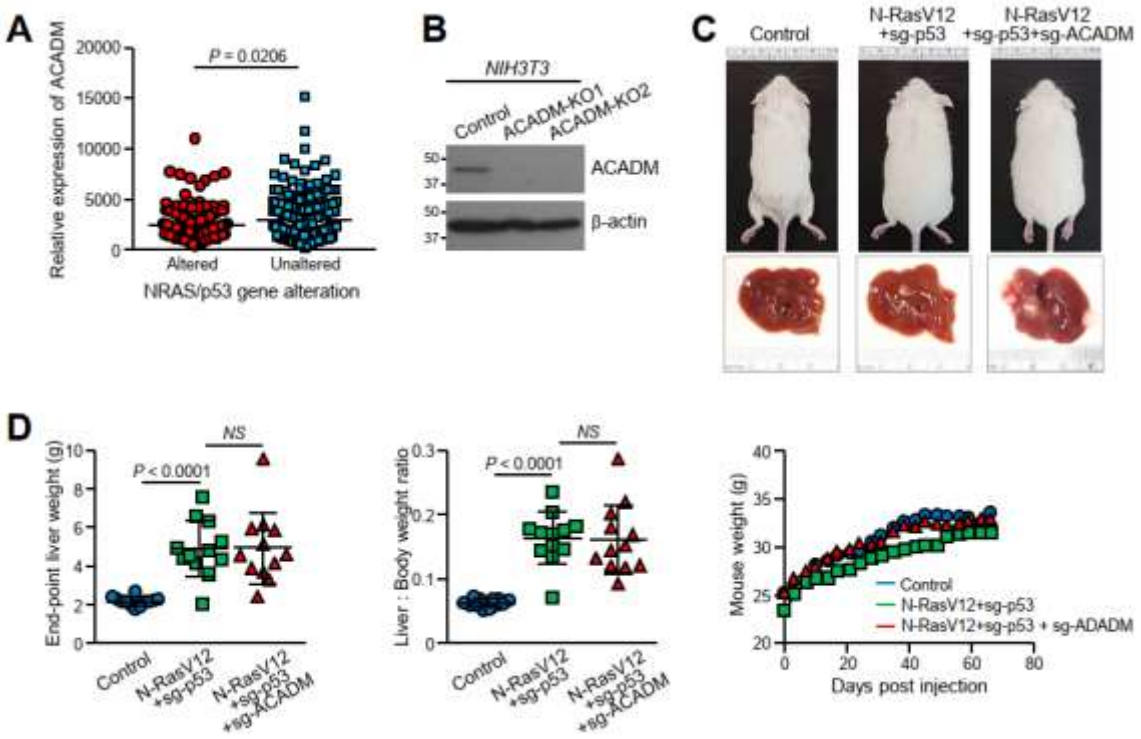

Supplementary Figure 5. Rationale for the choice of oncogene combination for hydrodynamic injection and the effect of ACADM-KO in mice.

(A) Data from TCGA revealed the decreased ACADM expression upon NRAS/TP53 gene alterations. (B) The knockout of ACADM (ACADM-KO1 and -KO2) were established in the mouse cell line NIH3T3 and confirmed by western blotting. (C) The livers excised from one mouse from each group at week 4 post-injection to observe tumour growth. (D) The end-point liver weight, liver:body weight ratio and mouse weight of mice injected with different oncogenes observed after hydrodynamics injection.

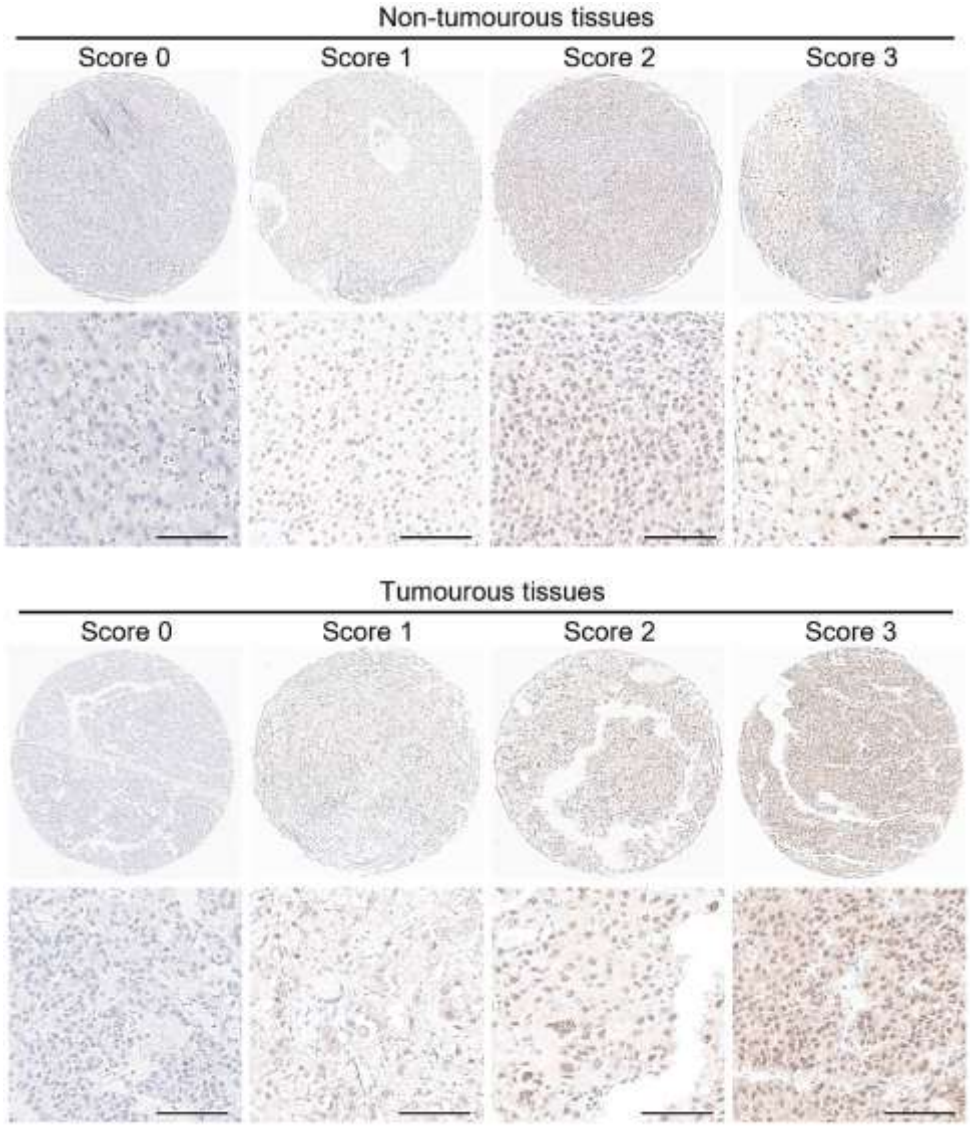

Supplementary Figure 6. Expression levels of SREBP-1 in tissue microarray tissues.

The different stain intensities of SREBP-1 as observed in non-tumourous and tumourous tissues, with the morphology of cells varying from the lowest to the highest score. Scale bar, 100 μm.

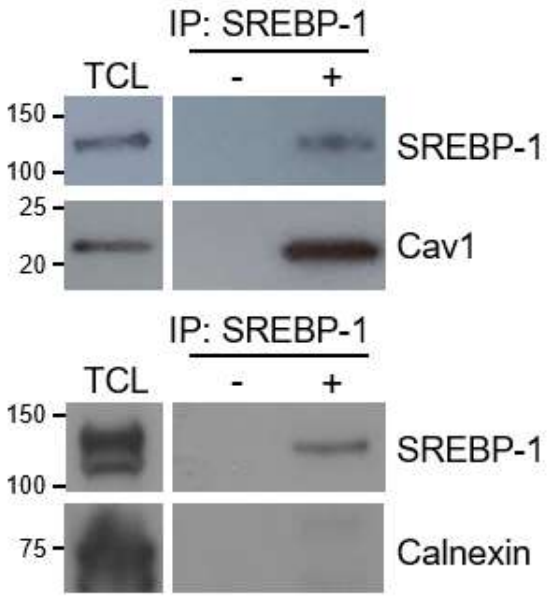

Supplementary Figure 7. Interaction between Cav1 and SREBP-1.

Total cell lysate of MHCC97L cells were immunoprecipitated with anti-SREBP-1 antibody and the immunoprecipitated protein lysate was subjected to immunoblotting using anti-SREBP-1, anti-Cav1 and anti-Calnexin antibodies. Calnexin, an ER protein, was included as a negative control.

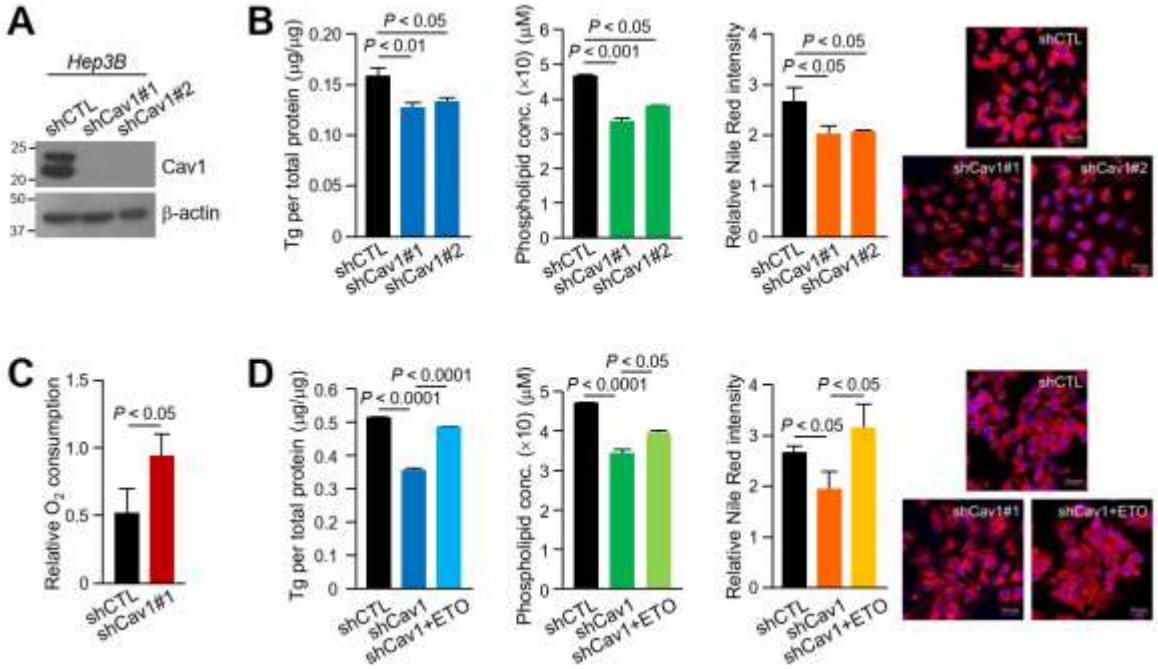

Supplementary Figure 8. Cav1 promotes HCC via its regulation in lipid metabolism in non-metastatic HCC cells.

(A) Western blot revealed the expression of Cav1 in Hep3B stable non-target control (shCTL) and Cav1 knockdown clones (shCav1#1 and #2). (B) The cellular triglycerides (Tg), phospholipids and Nile Red staining (scale bar, 50 μm) of the oil droplets in cells. (C) The fatty acid oxidation assay was used to determine the cellular respiration rate of HCC cells. (D) The addition of ETO to inhibit FAO restored the TGs, phospholipids and cellular lipids (scale bar, 50 μm) in shCav1 cells treated with ETO.

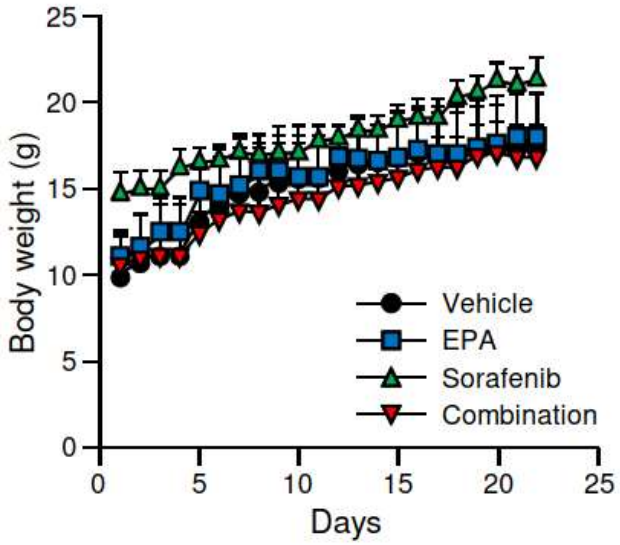

Supplementary Figure 9. Body weight of mice during EPA and sorafenib treatment.

Body weight of mice was measured daily over the course of the treatment period.

Supplementary Tables

Supplementary Table 1. Sequences of oligonucleotides used in the study.

Type	Clone	Sequence 5’ to 3’
shRNA	Human shCav1-1 (NM_001753.3-441s1c1)	CCGGGACCCTAAACACCTCAACGATCTCG AGATCGTTGAGGTGTTTAGGGTCTTTTT
	Human shCav1-2 (NM_001753.3-462s1c1)	CCGGGACGTGGTCAAGATTGACTTTCTCG AGAAAGTCAATCTTGACCACGTCTTTTT
	Human shACADM-61 (NM_000016.4-1396s21c1)	CCGGGCTGGCTGAAATGGCAATGAACTCG AGTTCATTGCCATTTCAGCCAGCTTTTTG
	Human shACADM-65 (NM_000016.4-1547s21c1)	CCGGGTGCAGATACTTGGAGGCAATCTCG AGATTGCCTCCAAGTATCTGCACTTTTTG
	Human shACADM-92 (NM_000016.4-1666s21c1)	CCGGCCGTGAACACATTGACAAGTACTCG AGTACTTGTCAATGTGTTCACGGTTTTTG
ORF cDNA	Human SREBP1 (NM_004176.4)	Identical with the GenBank sequence except for the point mutations not causing the amino acid variation
Primer	ACADM-1450-Kpn-F	GGTACCAATGTACTTTGTGCTCTTAGCTG
	ACADM+41-Bgl-R	GAAGATCTCGGTTGCGCTGAACGGTGGG
	ACADM-1450-F	AATGTACTTTGTGCTCTTAGCTG
	ACADM-950-R	GCTCGACTTCACAGGCTGCTC
	ACADM-540-F	AATTCCCAGAAGACAAAGTAGGG
	ACADM+41-R	CGGTTGCGCTGAACGGTGGG
sgRNA	Murine ACADM-KO-F	CACCGCTCGAAAGCGGCTCACAAGC
	Murine ACADM-KO-R	AAACGCTTGTGAGCCGCTTTCGAGC
Primer	Myco5	YGCCTGVGTAGTAYRYWCGC
	Myco3	GCGGTGTGTACAARMCCCGA

Supplementary Table 2. Antibodies used in the study.

Target	Source & Cat. No.	Isotype	Dilution	Application*
Cav1	BD Bioscience, 610406	Mouse	1:1000 and 1:100	WB, IHC and IP
Cav1	Cell Signaling Technology 3267S	Rabbit	1:1000	WB
ACADM	Abcam ab92461	Rabbit	1:10000 and 1:100	WB and IHC
SREBP-1	Santa Cruz Biotechnology sc-13551	Mouse	1:1000 and 1:100	WB, IHC and IP
β-actin	Sigma-Aldrich A5316	Mouse	1:5000	WB
α-tubulin	Sigma-Aldrich T9026	Mouse	1:1000	WB
c-Jun	BD Bioscience 610326	Mouse	1:1000	WB
CD31	Abcam ab28364	Rabbit	1:100	IHC
Ki-67	Dako M7240	Mouse	1:1000	IHC
p53	Invitrogen MA5-14067	Mouse	1:250	IHC
N-Ras	OriGene TA505835	Mouse	1:125	IHC
Calnexin	Affinity Bioreagents BF0515	Mouse	1:1000	WB

*WB = Western blot, IP = Immunoprecipitation and IHC = Immunohistochemistry.

Supplementary Table 3. Clinicopathological correlation of ACADM expression in HCC. P-value of < 0.05 was considered as statistically significant and marked with an asterisk (*).

		Cases with ACADM underexpression	Cases without ACADM underexpression	
Parameter	Category	T/NT ≤ 0.5	T/NT > 0.5	*P*-value
Sex	Male	22	12	1.000
	Female	10	5	
HBsAg	Positive	29	13	0.217
	Negative	3	4	
Cirrhotic liver	Cirrhosis	10	13	0.006*
	Normal & CH	22	4	
Cell differentiation by Edmondson grading	I & II	11	13	0.007*
	III & IV	21	4	
Tumour size	> 5 cm	22	6	0.035*
	≤ 5 cm	10	11	
Direct liver invasion	Present	12	5	1.000
	Absent	17	9	
Tumour nodule	≥ 2	5	2	1.000
	= 1	27	15	
Tumour encapsulation	Absent	20	9	0.541
	Present	11	8	
Tumour microsatellite formation	Present	13	3	0.123
	Absent	19	14	
Venous invasion	Present	16	3	0.034*
	Absent	16	14	
pTNM stages	I & II	13	13	0.013*
	III & IV	19	3	

HBsAg = Hepatitis B surface antigen and pTNM = Pathological Tumour-Node-Metastasis.